

POLITECNICO DI TORINO

Collegio di Ingegneria Biomedica

**Corso di Laurea Magistrale  
in Ingegneria Biomedica**

Tesi di Laurea Magistrale

**Estimation of Ground Reaction Forces  
During Running Based on Motion Sensors  
and Artificial Neural Networks**



**Relatori:**

Danilo De Marchi  
Brendan O'Flynn

**Correlatore:**

Salvatore Tedesco

**Candidato:**

Salvandra Di Salvo  
Matricola 242523

Ottobre 2018





# Prefazione

“Se vuoi aver successo nella vita, fai della perseveranza il tuo migliore amico, dell’esperienza il tuo saggio consigliere, della cautela il tuo fratello maggiore e della speranza il tuo angelo custode.”

[Joseph Addison]

Sono arrivato ad un altro traguardo importante della mia vita. Un’altra tappa che si conclude, ed è forse stata la più emozionante e gratificante. Si conclude con questo lavoro di tesi che ha caratterizzato l’ultimissima parte dei miei studi, un periodo passato in terra Irlandese che mi ha permesso di conoscere altre grandi persone, di interfacciarmi con altre culture e di arricchire ancora di più il mio bagaglio di esperienze.

Ho messo in questo lavoro tutto me stesso, poichè reputo questo settore della scienza fondamentale in quel processo di miglioramento della vita umana che è il fine ultimo dell’ingegneria biomedica. Ho studiato, in questi mesi e

negli ultimi anni, con la convinzione che questi strumenti possano davvero potenziare ciò che sono le abilità umane. Il mio lavoro non cambierà di certo il mondo, ma per me rappresenta un primo, timido passo verso l'uomo e il professionista che voglio diventare. Questa è la mia nuova sfida.



# Contents

<b>List of figures</b>	<b>vi</b>
<b>Abstract</b>	<b>ix</b>
<b>1. Overview</b>	<b>1</b>
1.1 Introduction to biomechanical analysis. . . . .	1
1.2 Running analysis. . . . .	3
1.3 Mechanic of the movement. . . . .	7
1.4 State of the art of the GRF measurement. . . . .	12
1.5 Aim of the thesis. . . . .	18
<b>2. Inertial sensors</b>	<b>20</b>
2.1 Introduction to the inertial sensors. . . . .	20
2.3 Gyroscope. . . . .	23
2.3 Accelerometer. . . . .	30
<b>3. Data mining</b>	<b>36</b>

3.1 Overview. . . . .	36
3.2 Neural networks. . . . .	37
3.3 State of the art. . . . .	53
<b>4. Data collection</b>	<b>58</b>
4.1 Data acquisition. . . . .	58
4.2 GRF waveform reproduction. . . . .	62
<b>5. Results</b>	<b>71</b>
5.1 Learning approach. . . . .	71
5.2 Outcome measures. . . . .	73
5.3 Results. . . . .	75
5.3 Future works. . . . .	77
<b>Conclusions</b>	<b>79</b>
<b>Bibliography</b>	<b>82</b>

# List of Figures

1.1	Free body diagram of an athlete during running.....	2
1.2	Running phases.....	4
1.3	Stance phase.....	5
1.4	Swing phase.....	6
1.5	Ground reaction force waveform during running.....	8
1.6	Mass-spring system of the running phase.....	10
1.7	Trends of the energy associated to the different body segments during running.....	12
1.8	Force platform.....	13
1.9	Instrumented treadmill.....	14
1.10	Motion tracking example.....	16
1.11	Xsens Forceshoes.....	17

2.1	Example of a transcharacteristic graph of a sensor .....	22
2.2	Mechanical gyroscope.....	25
2.3	Scheme of optical gyroscope.....	26
2.4	Vibration modes of tuning fork gyroscope.....	28
2.5	Mass-Damper-Spring system.....	30
2.6	Scheme of a capacitive accelerometer MEMS.....	32
2.7	Scheme of a surface acoustic wave accelerometer.....	33
3.1	Comparison between biological neuron and an artificial neural network structure.....	39
3.2	Artificial neuron model.....	40
3.3	Threshold function.....	42
3.4	Linear function.....	42
3.5	Sigmoid function.....	43
3.6	One layer neural network feed-forward.....	44
3.7	Multi-layer neural network feed-forward.....	45
3.8	Recurrent feed-forward network.....	45
3.9	Schematic of a perceptron.....	49
3.10	Linear separability in perceptrons.....	50
3.11	Schematic of multilayer perceptron.....	51

3.12 Complete insole detailing sensor locations.....	54
3.13 Collected and simulated GRF in both configurations.....	55
3.14 Schematic of the system with the two concatenated ANN.....	56
3.15 Ann model that represents one of the best mapping tool for kinematic data.....	57
4.1 Actigraph GT9X.....	59
4.2 Actigraphs wore on the shanks.....	60
4.3 Running on the treadmill during trials.....	61
4.4 Two mass-model.....	63
4.5 Lower limb motions.....	68
4.6 Different schematic graphs of the lower limb mass $m_1$ .....	69
4.7 GRF recreated via Clark's method.....	70
5.1 Graph of the network realized.....	72
5.2 Table with MAE and R for the different ANN topologies.....	75
5.3 Table with MAE and R of the network with 30 neurons in the final testing.....	76

# Abstract

Analysis of running mechanics, especially of ground reaction forces (GRFs) provides an indication of the loads to which the body is subjected at each foot-ground contact, and more importantly it can be linked to the performance outcomes and the risk of injury. This type of analysis has traditionally been limited to a gait laboratory using either force plates or instrumented treadmill. The aim of this study is to investigate the potential for wearable motion devices to be employed, in combination with artificial neural networks (ANNs), for the estimation of vertical ground reaction forces (vGRF) at different speeds running. More in details, several ANNs with different number of neurons in the single hidden layer were implemented, and were used in combination with a system of wearable Inertial Measurement Unit sensors (IMUs). The different ANNs were developed and validated via a Leave One Subject Out - Cross Validation (LOSO – CV), in terms of mean absolute error (MAE) and Pearson's correlation coefficient (R).

Results are promising and the present work proves the emergent ability to obtain GRFs from wearable device can lead to an accurate and low-cost quantification of the training stress and competition demands in running also on-the-field.





# Chapter 1

## Overview

### 1.1 Introduction to biomechanical analysis

Human gait analysis encloses the identification of biomechanical walking or running gait parameters, and is a crucial tool in many applications, including medical diagnosis injury prevention and professional sports.

The gait analysis is, thus, a significant clinical tool, because the movements for the walking and running phases are the interaction of three main physiological systems: the nervous system, the muscular-skeletal system, and the sensorial system [1].

In particular, running has always been an activity investigated by a number of researchers, because a precise biomechanical analysis during running can

## CHAPTER 1. INTRODUCTION

give a number of important parameters to potentially predict injuries and to increase performances of athletes.

Unfortunately, such analysis is complicated when the measurements must be performed during training or a competition, as it is not easy to set up an athletic track with cameras, force platforms and other instruments needed to measure the biomechanical parameters.

Indeed, it is important to figure out every details of the human movement, and, more specifically, to identify biomechanical inefficiencies and help identify running related problems that may result in injury.

Ground Reaction Forces (GRFs) are important to analyse, because they can give a good indication of how is made the contact between the patient foot and the ground (figure 1.1).

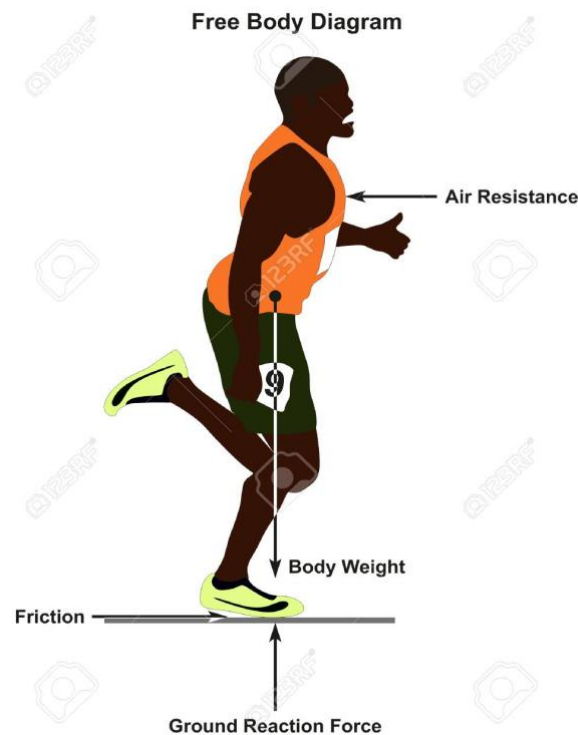


**Fig. 1.1** Free body diagram of an athlete during

Typically, the most investigated aspects of running are the contact time interval ( $t_C$ ), flight time ( $t_V$ ), step rate ( $f$ ) and vertical displacement of the mass center ( $\Delta z$ ).

These parameters can be recorded directly using video analysis (e.g. via Optical Motion Capture system) or force platforms, as will be discussed in 1.4.

## 1.2 Running analysis

The present paragraph will discuss the biomechanics of running and the phases that characterize this activity.

The running cycle represents as all the movements between two consecutive contact moments of the same foot with the ground. The running cycle can be divided in two main phases: “Stance phase” and “Swing phase” (figure 1.2).

The stance phase starts with the contact between the foot and the ground and finishes with the movement of bending/extension of the limb in support; this represents the 40% of the whole cycle.

The second one is the oscillating phase in which the foot is not in contact with the ground; this phase represents the 60% of the cycle. During the running phases it is possible to identify also a “Floating phase”. It is characterised by the recovery movement performed by the lower limbs in

## CHAPTER 1. INTRODUCTION

order to guarantee the correct alternation between the two legs and it represents the remaining 30% of the running phase.

As evident from figure 1.2, during running there is no moment in which both of the feet are touching the ground (known as double support).

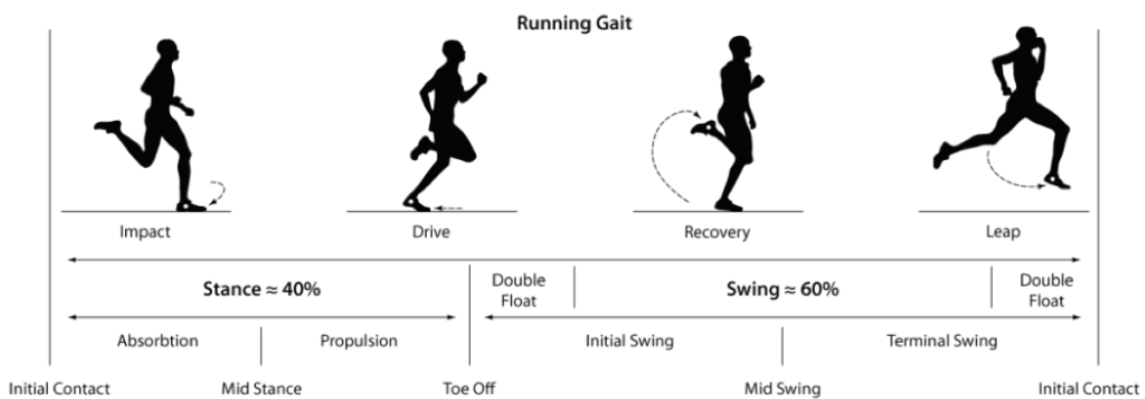


Fig. 1.2 Running phases

### 1.2.1 Stance phase

The phase in which the foot is in contact with the ground is the most important one in order to understand the potential injuries caused by running due, for example, to continuous impacts with unsuitable terrains.

This phase can be differentiated in three different moments (figure 1.3):

1. Amortization moment or contact, e.g. the moment in which the foot touches the ground (foot strike) and impact amortization due to the action of the sural triceps.

During this phase the elastic component of the foot is used. The support foot is in front of the centre of gravity of the body.

2. Single support moment, namely the linear advancement and horizontal of the pelvis. In this phase, the foot is perfectly along the same axis with the centre of gravity (midsupport), the muscles are contracted to maintain the stability of the body.
3. Boost moment, e.g. the straightening of the support limb (take off), which produces the necessary acceleration for the detachment of the foot from the ground. The foot is behind the centre of gravity. The muscles use the elastic force to push the body forward (distension of the leg).



Fig 1.3 Stance phase

## CHAPTER 1. INTRODUCTION

### 1.2.2 Swing phase

The swing phase is the phase in which the foot is not in contact with the ground. This phase is included between the moments of ‘take off’ and ‘foot strike’ and is divided in 3 sub-phases (figure 1.4):

1. *Follow through*, such sub-phase starts with the raising of the limb from the ground until the position of maximum knee flexion
2. *Forward swing*, time period that starts when the knee is at maximum flexion and continues until the beginning of the flight phase.
3. *Foot descent*, oscillating period of the limb that follows the end of the flight phase that establish the end of the swing phase and the beginning of the stance phase.

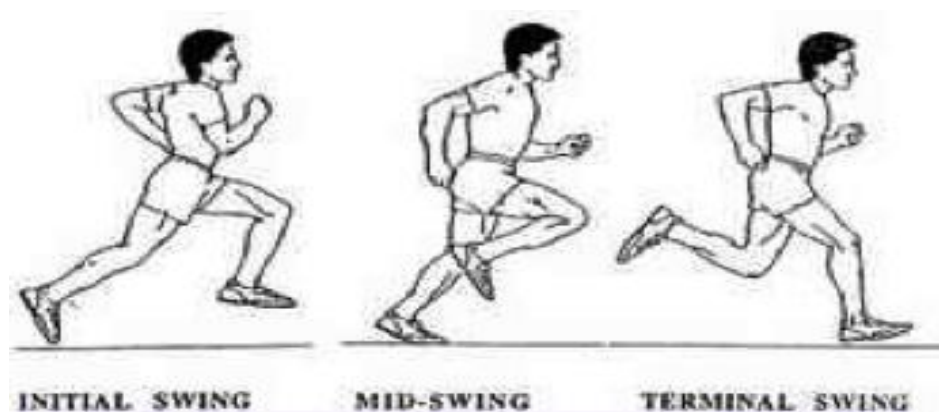


Fig. 1.4 Swing phase

### 1.2.3 Floating phase

Once that the limb is detached by the ground, the limbs, with the pelvis as fulcrum, act in opposite direction; the foot of the free limb is moving rapidly in front.

The foot of the limb in boost is going away from the pelvis. In leaving the ground, the foot is subjected to an acceleration and the limb flexes to the knee.

## 1.3 Mechanics of the movement

This paragraph gives a description of the ground reaction forces associated with running.

The human body can be divided in several segments; when each segment is moving, the chemical energy is converted in mechanical energy by the muscles and what is obtained is Work.

The mechanical energy associated to every segment are kinetic energy ( $E_{k,i}$ ) and potential energy ( $E_{p,i}$ ) and are described as follows:

$$E_{k,i} = \frac{1}{2}m_i v_i^2 + \frac{1}{2}I\omega_i^2 \quad (1)$$

$$E_{p,i} = m_i g_i h_i + \frac{1}{2} k_i x_i^2 \quad (2)$$

Where the kinetic energy is composed by a term related to the linear velocity ( $v_i$ ), the mass of the segment ( $m_i$ ), and by a second term that is related to the energy associated to rotation velocity ( $\omega_i$ ) of the segment and the inertial moment ( $I$ ).

The two potential energy terms are related to gravitational potential energy ( $g_i$  is the gravitational acceleration,  $h_i$  is the height of the segment relative to the ground) and the elastic potential energy ( $k_i$  is the elastic constant,  $x_i$  is the stretching) regarding the tendons and muscles compression and decompression, which, during the movement, behave as springs, enabling to recover part of the kinetic energy dissipated during a deceleration of the segment.

The image below represents divides the ground reaction force waveform during running in two parts: absorption and generation of energy.

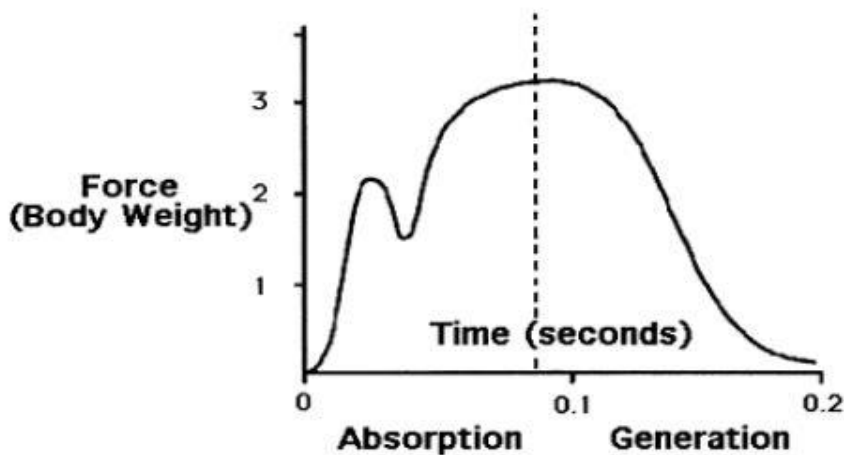


Fig. 1.5 Ground reaction force waveform during running

Concerning the velocity and the displacement of a body segment, they can be divided in velocity (and movement) of the mass centre ( $v_{COM}$ ) and the velocity (and movement) of the particular part compared to the mass centre ( $v_{rel}$ ):

$$v_i = v_{COM} + v_{r,i} \quad (3)$$

The total amount of energy is equal to the sum of each segment of the human body, and every segment has a part of kinetic energy and potential energy:

$$E_{tot} = \sum_{i=1}^N (E_{k,i} + E_{p,i}) \quad (4)$$

With  $N$  being the number of body segments.

Dividing the components relative to the mass centre is possible to obtain:

$$E_{tot} = MgH_{COM} + \frac{1}{2}Mv_{COM}^2 + \sum_{i=1}^N \left( \frac{1}{2}m_i v_{r,i}^2 + \frac{1}{2}I_i \omega_i^2 \right) \quad (5)$$

Where  $M$  is the body mass and  $H_{COM}$  is the height of the mass centre. Theoretically during the running phase with a constant velocity on flat ground, the variation of  $E_{tot}$  is oscillating with a period equal to the step period . The energy between the different steps is always constant.

## CHAPTER 1. INTRODUCTION

However, this is an ideal case not present in the human body.

Normally tendons are comparable to elastic energy accumulator and, furthermore, the muscles dissipate energy even in the negative force case (opposite direction). Considering this in a model is complex, therefore the classical approach is to neglect the negative work.

To visualize the system, the running phase can be described easily through a mass-spring system (figure 1.6):

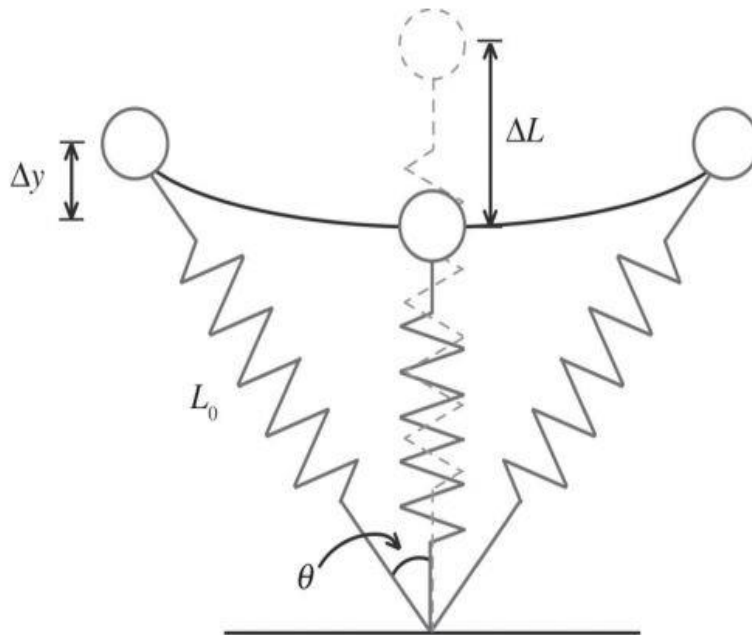


**Fig. 1.6** Mass-spring system of the running phase

The lowering of the mass centre in the first phase corresponds to a loose of potential energy (stored into the spring); afterwards the spring releases the energy stored earlier, in order to lead the mass to the initial position. From this instant the mass centre will have the classical ballistic movement determined by the initial velocity.

The use of the spring involves the linear relation between the leg lowering and the ground reaction forces.

Reconsidering equation 5, it is possible to distinguish two terms:

- External work ( $W_{ext}$ )

$$W_{ext} = MgH_{CoM} + \frac{1}{2}Mv_{CoM}^2 \quad (6)$$

- Internal work ( $W_{int}$ )

$$W_{int} = \sum_{i=1}^N \left( \frac{1}{2}m_i v_{r,i}^2 + \frac{1}{2}I_i \omega_i^2 \right) \quad (7)$$

It is possible to think external work as the necessary work to raise up and accelerate the mass, while the internal work is the one necessary for the movements related to the CoM.

From these concepts, it is possible to compute the mechanical power e.g. :

$$P_M = \frac{W_{tot}}{t} = \frac{W_{ext} + W_{int}}{t} \quad (8)$$

Where  $t$  is the duration of the period of interest.

In the case of running with a constant velocity, it is possible to compute the following forces balance:

$$\vec{F} = G\vec{R}F + \overline{B\vec{W}} \quad (9)$$

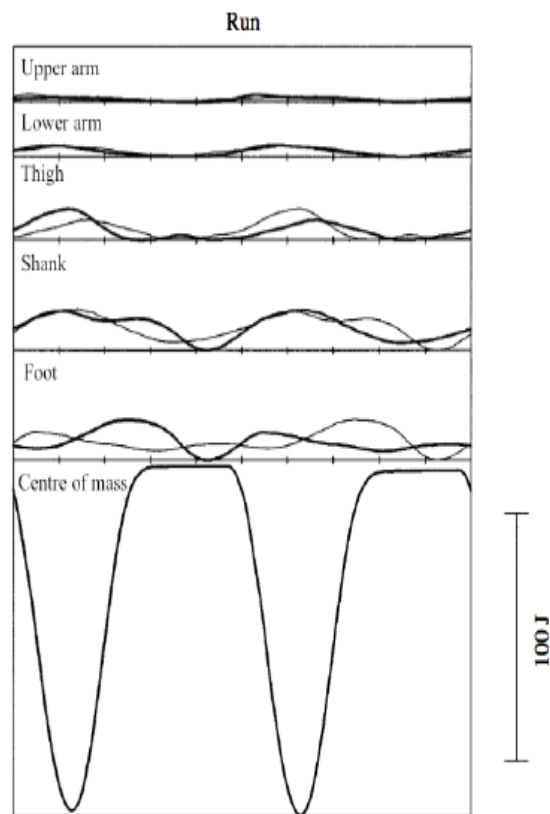


**Fig. 1.7** Trends of the energy associated to the different body segments during running

Where  $\vec{GRF}$  represents the Ground Reaction Forces and  $\vec{BW}$  is the gravitational force applied to the body weight. Given the absence of the acceleration during the gait the mean value of  $\vec{F}$  will be null [2] (figure 1.7).

#### 1.4 State of the art of the GRF measurement

The present paragraph will provide details on the currently available technologies for the estimation of GRF.

### 1.4.1 Instrumented treadmill and force platform

Force platforms represent the gold standard technology for estimating GRF. Those force platforms are based on strain gauge, piezoelectric and piezoresistive sensors and have to be positioned on the ground in order to measure the force applied by the patient during a specific test. (figure1.8)



**Fig.1.8** Force platform

However, despite the excellent results, force platforms also show a number of shortcomings, e.g:

- Not portable;
- Expensive;
- Requiring a laboratory and trained personnel;
- Ability to capture a single stride per test.

To simplify the data collection, allowing for the data acquisition of hundreds of steps in a single experiment, instrumented treadmill (figure 1.9) are also adopted which, however, are even more costly.

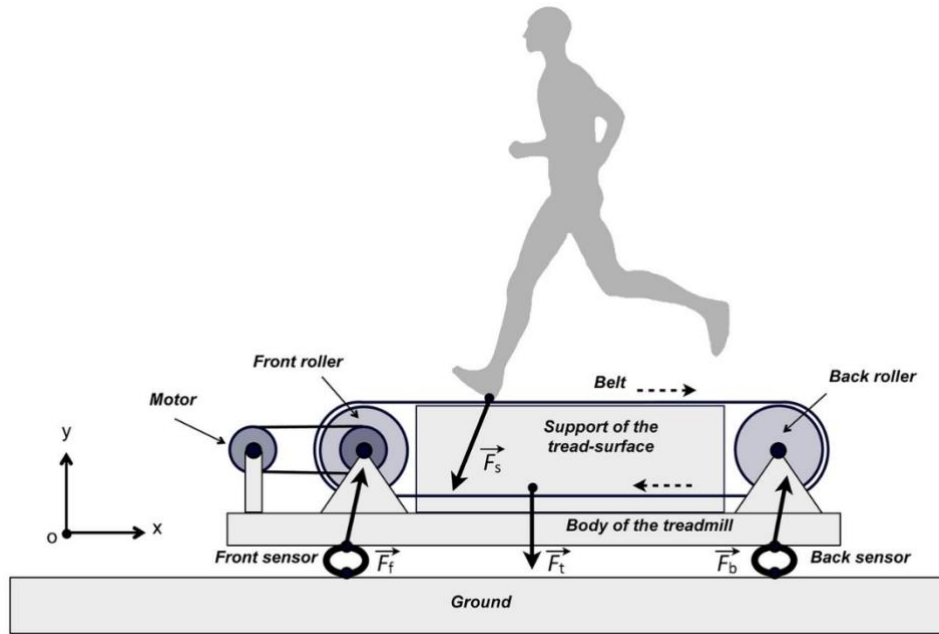


Fig. 1.9 Instrumented treadmill

### 1.4.2 Motion Capture

The Motion Capture system (or Mocap) is a technology for the data collection of the human movements in order to use them for 3D analysis on a computer. Motion Capture systems are typically realized using one of the following technologies: magnetic and optical.

**MAGNETIC SYSTEM** The magnetic systems use sensors that are placed along body segments to measure the magnetic field intensity generated by a transmitter. The sensors are in communication with an electronic control unit that correlates the signals generated within the field.

The electronic unit control are connected with a computer that uses a software to represent the sensor position and orientation in the 3D space.

**OPTICAL SYSTEM** This system consist of a camera set which are recording the area where the subject is moving. In general the cameras are calibrated and fixed. The patient movement is computed via imaging data elaboration.

There are three categories of optical motion capture:

- *Markerless optical systems* consist of systems that are able to recognize automatically the different body segments on the taken pictures via image processing, then computing the position and the orientation;
- *Optical systems with passive markers* combine the using of flash and reflective markers in order to generate images with high contrast in which is easy to detect the marker positions (figure 1.8);
- *Optical systems with active markers* are very similar to the passive ones, but in this case the markers are composed by coloured LED which issue light itself, so an external illumination it is not needed as in the previous case [3].



**Fig. 1.10** Motion tracking example

The motion system do not measure GRF by themselves but are typically associated with force platforms. However, there are a number of papers where researchers aim to estimate GRFs from only a MoCap (Motion capture) system, which however does not eliminate most of the issues reported in terms of lab-constraint and cost [1].

### *1.4.3 Wearable solutions*

To overcome the abovementioned limitations of gait measurement in laboratory environment , several techniques have been developed in the last few years to measure or estimate GRF using wearable sensors.

The techniques can be divided in three categories based on the type of measured parameters:

- Methods based on measurements of kinematic data use a human body dynamic model to estimate GRF(t), GRM(t) from acceleration of different body segments. The pro of this method consist of using inexpensive and wearable tools, such as inertial measurement units (IMUs).
- Methods based on measurements through plantar pressure that uses a matrix of insole pressure sensors in order to measure the pressure under each foot perpendicular to the contact surface.
- Method based on force measurement that measure directly the tri-axial GRF(t) and CoP(t) (centre of pressure) under each foot, using load cells. (figure 1.11)



**Fig. 1.11** Xsens Forceshoes are very accurate, on the other hand they are bulky and expensive

## *CHAPTER 1. INTRODUCTION*

The methods based on IMUs may enhance the direct measurements of the GRF, furthermore there is no need to put a rigid material under the foot as in the load cell method, which could affect the running quality of the subjects.

### 1.5 Aim of the thesis

The aim of the thesis is to develop an artificial neural network able to predict Ground Reaction Forces in athletes during running.

To predict Ground Reaction Forces, we will use a set of wearable sensors (IMU-inertial measurement unit) that measures parameters such as acceleration and radial velocity of different body segments; afterwards it is applied a feature selection procedure to the data, so the ANN will be trained by using input parameters represented by these features and the target parameters represented by the ground reaction forces obtained by an algorithm which recreates realistic force plate measurements. The ANN, then, will find the correlation between the IMU-data and target-data (force plate) in order to be able to predict the GRFs.

The structure of this study starts with the description of the functioning of inertial sensors used. Chapter 3 describes the Artificial Neural Network that enhances the prediction of the GRF using only the inertial data. Chapter 4 focuses mainly on the protocol implemented for the Data collection and the

## *CHAPTER 1. INTRODUCTION*

force platform waveform simulation method. Chapter 5 describes testing and validation of the neural network on the running phase data and finally chapter 6 draws conclusions and possible future applications related to this study.

# Chapter 2

## Inertial sensors

### 2.1 Introduction to the inertial sensors

The sensors used to measure motion parameters in athletes are Inertial Measurement Units sensors (IMU). They are electronic devices that integrate multi-axis combination of:

- tri-axial gyroscopes;
- tri-axial accelerometers;

Usually, a tri-axial magnetometer is added to the platform, this configuration is called MARG (magnetic angular rate and gravity). The orientation information of the sensor, given the initial conditions, are computed by the integration of the measured angular velocity and are described through Euler angles.

There are several parameters that characterize the quality of sensors and are as follows:

- Input and output values;
- Accuracy;
- Resolution;
- Linearity;
- Offset;
- Precision;
- Sensibility;
- Stability;
- Response time;

**INPUT AND OUTPUT VALUES** To be confident about input data (IR - input range) it is important to obtain reliable systems. The variability of the input has to be within sensor IR.

The output values (OR – output range) are fundamental for the sizing of the whole measurement chain (sensors, conditioning blocks, ADC exc.).

**ACCURACY** this parameter is strongly connected to the knowledge of the trans characteristics of the sensor (figure 2.1). The trans characteristic is a graph that matches every value of the input to another one of the output

## CHAPTER 2. INERTIAL SENSORS

*RESOLUTION* is defined as the smallest increment of the input recognised by the sensor through a variation perceptible of the output.

*LINEARITY* the deviation of the trans characteristic curve from the linear condition is called linearity. High linearity is fundamental to obtain correct estimations and especially stability of the measurement chain.

*OFFSET* the offset error is the value not null of the sensor output obtained in correspondence of null input.

*PRECISION* the precision, called also repeatability, of a sensor is the capacity to provide similar outputs, with the same input.

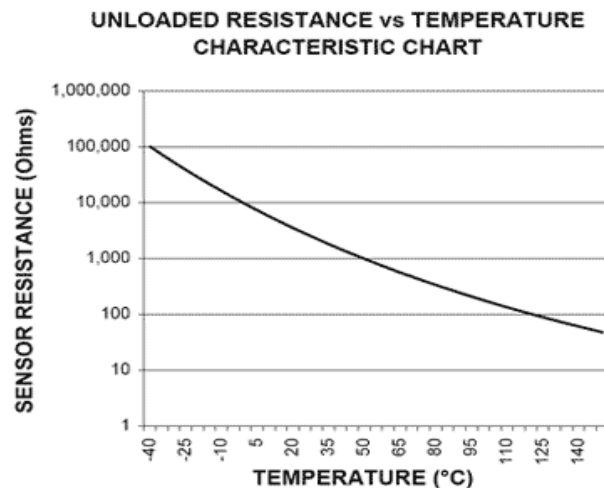


**Fig. 2.1** Example of a transcharacteristic graph of a sensor that varies its Resistance depending on the external temperature

*SENSIBILITY* sensibility is defined as the ratio between the output variation and the input variation. It is possible to describe it as the gain of the sensor or more simply the trans characteristic pendency.

*STABILITY* It represents the capacity to not modify the trans characteristic itself of the sensor. Several contributes may lead to decrease the stability, as the temperature, the aging of the components and other factors that are matched with the particular sensor realization.

*RESPONSE TIME* the response time is the time used by the sensor to switch from one output state to another one, caused by a variation of the input. It is possible to notice that the time response is strongly connected to the band width of the measurement chain [4].

## 2.2 Gyroscope

### 2.2.1 *Structure and working principles*

The gyroscope is a device able to measure the angular velocity of a mass. There are several types of gyroscopes that work through different working principles, and the most used are three [5]:

- Mechanical gyroscopes

## CHAPTER 2. INERTIAL SENSORS

- Optical gyroscopes
- MEMS gyroscopes

**MECHANICAL GYROSCOPE**      the mechanical gyroscopes are based on the conservation of the angular moment of the body.

A mass in rotation with an high angular velocity  $\omega$  is supported by cardan joints, a rotation of the support does not drag with itself the rotating mass that tends to hold the proper orientation. Measuring the relative angles between mass and joints enables to compute the asset of the sensor, as illustrated in figure 2.2.

Supposing  $\omega$  and the associated angular moment are along the x direction, the application of a couple along the y axis causes a precession movement around z axis with an angular velocity  $\Omega$ .

This phenomenon is exploited for the estimation of  $\Omega$  and z is named as sensing axis.

According to the second Newton's law, a couple applied to the rotating mass exists if there is an angular moment variation  $L$ . Such couple leads to rotate the mass around an axis that is perpendicular to both  $L$  and the couple itself. Measuring the position variation yielded, allows the estimation of  $\Omega$ .

This type of gyroscope is subjected to several problems due to using mechanical organs for metrologic activity, such as:

- Sensibility to mechanical variations.

- Warm up time (time that the system spend to be in operating conditions).
- Sensibility and deformations due to the temperature and components usury problems.

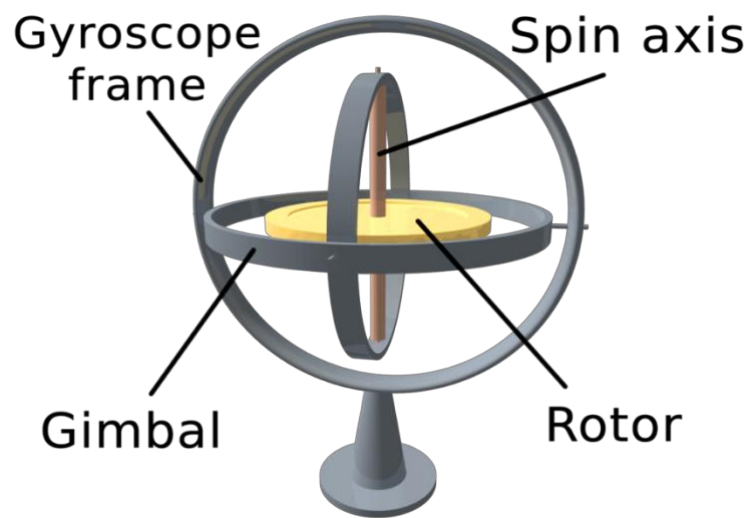


Fig 2.2 Mechanical gyroscope

**OPTICAL GYROSCOPE** The optical gyroscopes (figure 2.3) are based on the Sagnac effect. Two light beams are passed within a optical fibre ring in opponnet verse. In the case of a rotating ring, the two beams are subject to two different length waves: the beam that is moving towards the rotating direction of the ring is subject to a longer path.

The two beams afterwards are combined together, the resulting interference is strongly affected by the ring rotating velocity. These gyroscopes are very

precise and they do not have typical mechanical gyroscope problems due to moving organs.

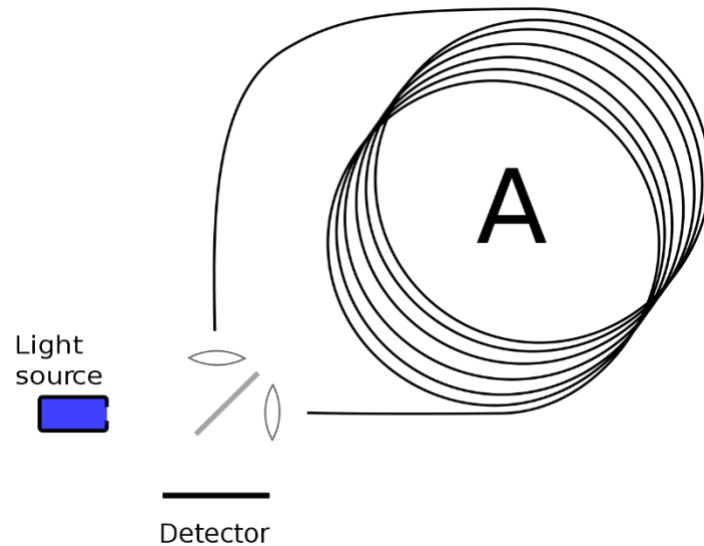


Fig. 2.3 Scheme of optical gyroscope

**MEMS GYROSCOPE** Some MEMS (Micro ElectroMechanical System) gyroscopes are based on the Coriolis effect. A mass in movement with a linear velocity  $v$  described in a not inertial reference system rotating with an angular velocity  $\omega$  is subject to an apparent force due to:

$$F_c = -2m(\omega \times v) \quad (10)$$

There are different realizations based on the principle described. The MEMS vibrating mass gyroscopes are an example of this, or the tuning fork gyroscope.

The first category has two masses kept in vibration along an axis (named drive axis), the oscillating movement presents a sinusoidal velocity  $v$  (for simplicity, the drive axis will be the x axis). In presence of an angular velocity  $\omega$  along z, it is possible to obtain two forces along y but with an opposite sense applied to the vibrating mass.

It is possible to obtain two forces along y but in opposite directions applied to the vibrating masses. It is possible to obtain an oscillating movement along y axis as well and its measurement through capacitive estimation makes possible to compute the angular velocity  $\omega$ .

The latter category, tuning fork gyroscope (figure 2.4), is similar. The forks are used as vibrating mass, supposing along y axis, a rotation with a velocity  $\omega$  around x axis causes the creation of two forces along z axis. These forces generate a moment only if the two tuning forks vibrate in opposition. The couple yielded tend to rotate the fork gyroscope support, allowing the estimation of  $\omega$ .

The strengths of MEMS realizations are:

- Sizes and reduced weights;
- Low power consume;
- Robustness;
- Inexpensive

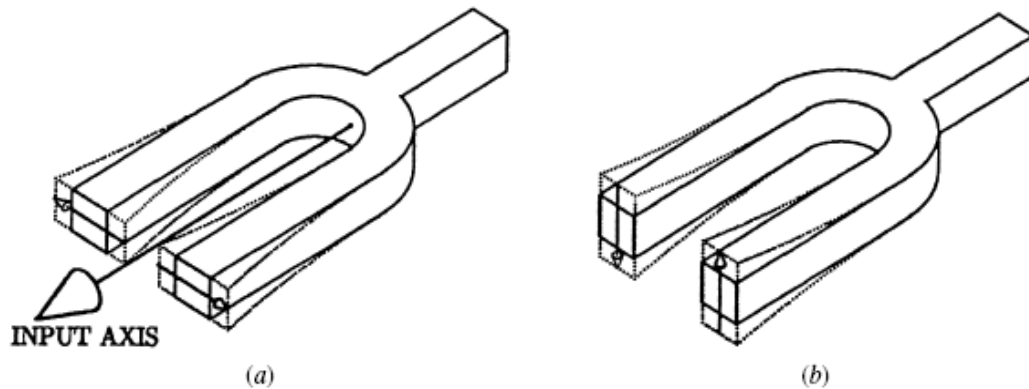


Fig. 2.4 Vibration modes of tuning fork gyroscope: (a) input mode; (b) output mode

### 2.2.2 Errors

The main errors that affect the measurements obtained through MEMS gyroscopes are [6]:

- Constant bias
- Angle random walk
- Bias stability
- Temperature effects
- Calibration errors.

**CONSTANT BIAS** The measurements obtained are affected by a constant offset error, called constant bias. It affects every measurement carried out and if it is integrated over time leads to a linear error:

$$\theta(t) = \epsilon \cdot t \quad (11)$$

It is possible to estimate this error computing an average of the results obtained over an extended time period with a firm sensor. At this point, compensating the next estimations is simple: it is enough to subtract the bias to the gyroscope output  $\epsilon$ .

**ANGLE RANDOM WALK** The MEMS gyroscope output is always disturbed by a thermal-mechanical noise that varies faster than the sensor sampling rate, thus it is possible to approximate this noise as a white Gaussian noise, with a null average and null correlation, overlying to the measurements. It does not cause an offset error, but an increasing of the standard deviation.

**BIAS STABILITY** The bias error can change along the time due to flickering, or flicker noise, of the electronic organs inside the instrument. Such noise has a spectrum inversely proportional to the frequency, and its effects can be noticed especially at lower frequency, because at higher frequency is hidden by the white Gaussian noise.

**TEMPERATURE EFFECTS** Temperature variations of the sensor and its work environment cause a bias variation. Estimating this change is not easy

## CHAPTER 2. INERTIAL SENSORS

and that is the reason why a number of IMUs involves temperature sensor within the sensor itself, in order to correct possible fluctuations due to temperature changing.

**CALIBRATION ERRORS** Calibration errors include: non linearity errors of the gyroscope transcharacteristics, axis alignment errors and scale adjustment errors. Such errors are correctable through a good calibration of the sensor or by using corrective factors.

### 2.3 Accelerometer

#### 2.3.1 Structure and working principles

An accelerometer is a device that measures changes in gravitational acceleration. Accelerometers are used to measure acceleration, tilt and vibration in numerous systems .

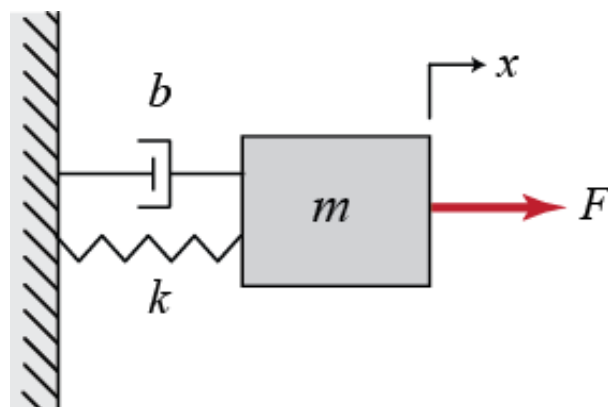


Fig. 2.5 Mass-Damper-Spring system

A typical model to describe such sensor is the Mass-Damper-Spring (figure 2.5), which has a transfer function given by:

$$H(s) = \frac{x(s)}{a(s)} = \frac{1}{s^2 + s\frac{b}{m} + \frac{k}{m}} \quad (12)$$

An accelerometer can be represented as a proof mass  $m$  suspended by deformable support, which is similar to a spring with an elastic constant equal to  $k$  and a damper with a damping coefficient equal to  $b$ .  $x(s)$  represents the Laplace transform of the deviation from the reference position,  $a(s)$  represents the acceleration transform of the sensor [8].

Such device is encapsulated in a rigid block. An external force applied to the sensor causes a compression or an extension of the spring; measuring this deformation makes possible to estimate the acceleration.

There are different types of accelerometer, with different working principles:

- Capacitive accelerometer (figure 2.6);
- Piezoresistive accelerometer;
- *Surface acoustic wave* accelerometer.

The first one measures the acceleration through the capacitance variation of its armatures, which change their position depending on the external

acceleration; the strengths of such solution are: high sensibility, low cost and low power dissipation, noise rejection [7].

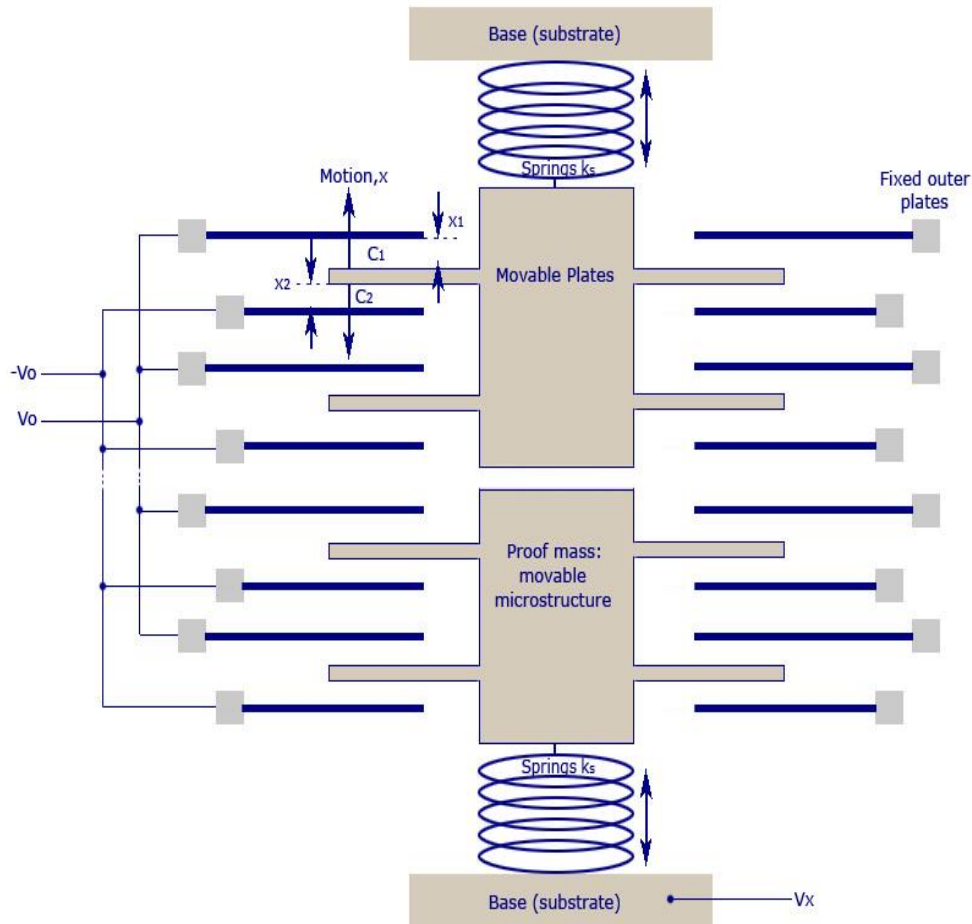


**Fig. 2.6** Scheme of a capacitive accelerometer MEMS

The second one measures the variation of resistance due to the supports deformation of the proof mass (called also piezoresistive beam). It presents a structure and a fabrication process that are not complex, but on the other hand it is really sensible to the thermal effects.

The third one (figure 2.7) uses the resonance frequency of a small piezoelectric element bonded to a cantilever stuck with a proof mass positioned on the free extremity. An acceleration applied to the mass causes a deformation of the rod that then modify the resonance frequency of the element [8].

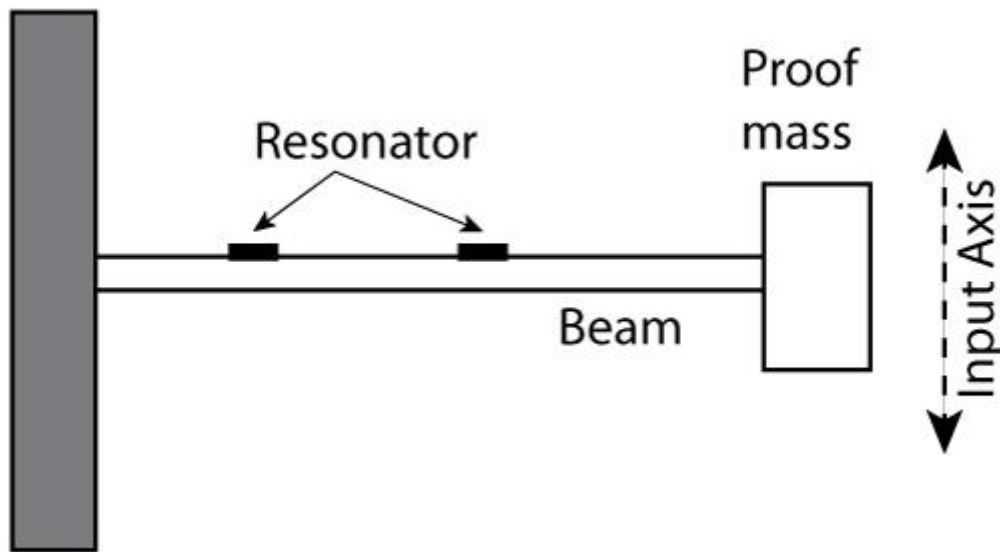


Fig. 2.7 Scheme of a surface acoustic wave accelerometer

### 2.3.2 Errors

The acceleration can be used to determine, through numerical integration, position and linear velocity of the sensor. Possible measurement errors, although limited, cause a rapid information deterioration about position and velocity computed.

The main errors, as reported in [9], are the following:

- Costant bias

## CHAPTER 2. INERTIAL SENSORS

- Velocity random walk
- Bias stability
- Temperature effects
- Calibration errors.

**COSTANT BIAS** As for the gyroscope, the bias is an offset error that varies from the “true value”. Defining the bias as “ $\epsilon$ ”, the error contribution regarding position estimation (integrated twice) is:

$$x(t) = \epsilon \frac{t^2}{2} \quad (13)$$

The velocity estimation will have a linear contribution.

**VELOCITY RANDOM WALK** Accelerometer output is always disturbed by a white noise with null correlation and average, overlapped to the measurements.

Such noise involves an increment of the standard deviation of the estimations, which is proportional to the square root of the integration time.

**BIAS STABILITY** It is caused by the flicker noise, which exists within the electronic device that tends to change continuously the sensor derive; it is possible to claim that the bias stability for an accelerometer describes how

much the sensor bias can change during a specific interval, with prefixed condition.

**TEMPERATURE EFFECTS** Another typical error is the error due to thermal effects: a temperature variation could modify the resistance or capacitance estimated.

For this reason several accelerometers involve, within the device, temperature sensors to correct the influence of  $T$ .

**CALIBRATION EFFECTS** Calibration errors are mainly affected by the non-perpendicularity of accelerometer axis.

# Chapter 3

## Data mining

### 3.1 Overview

To define synthetically Data Mining (DM), it is useful to report some definitions:

- *DM is the not banal extraction of implicit information, previously unknown and potentially useful through the use of different technical approaches (Frawley, Piatetsky-Shapiro and Matheus).*
- *DM is the research of relations and global models that are present in big database, but that are hidden in the big data amount, as the relationships between patient's data and their medical diagnosis. These relations represent a precious knowledge of the database and,*

*if the database is a loyal mirror, of the real world contained within itself (Holsheimer and Siebes).*

The increasing demand to manage data in the actual society of the information has pointed out the necessity to have instruments to analyse them, indeed the big quantity of data establishes a good informative potential that enable the definition of better decisions and actions. Data mining is not a simple statistic analysis but is more a procedure that involves one or more computational learning techniques to analyse and to extract knowledge from data within a database and it is then a learning strategy with an inductive nature that builds model to detect hidden pattern within data.

## 3.2 Neural networks

One of the most important and most famous data mining tools is the Artificial Neural Network (ANN) [9].

An ANN is a mathematical model that attempts to simulate the functional aspects and the structure of biological neural networks (figure 3.1) . It consists of units, called artificial neurons, which are joined by weighted connections, called synapses. Information can be treated using a connectionist method to computation: this means that tasks are not

### *CHAPTER 3. DATA MINING*

accomplished solving a deterministic structure of processes, but with a multitude of parallel and local processing involving all the units. These features are important as:

- This kind of structure enhances to process large amounts of data with great precision. They are rather independent to every assumption on data's distribution and interaction among components. They are particular statistical systems with a great robustness to noisy, incomplete or totally missing inputs;
- If some units do not work properly, the network could be affected by a degradation of the level of its performances, but almost never arrests its ongoing process.

Relative disadvantages are instead:

- The model generated by ANNs, although very effective, cannot be described with an analytical approach: results must be taken as they come and neural networks have to be considered as black boxes. It is not possible to comprehend how certain inputs cause

certain outputs, thus the only manner to achieve a performant ANN is to start from a set of well-chosen statistical data;

- In the case of a complex problem, the quantity of data necessary to design a correct ANN is very high and the computation of the network parameters needs an increasing computer effort. Mathematical models that allow to define the finest network structure are not available yet, so the final result is obtained with heuristic methods that heavily rely on the experience of their creator.

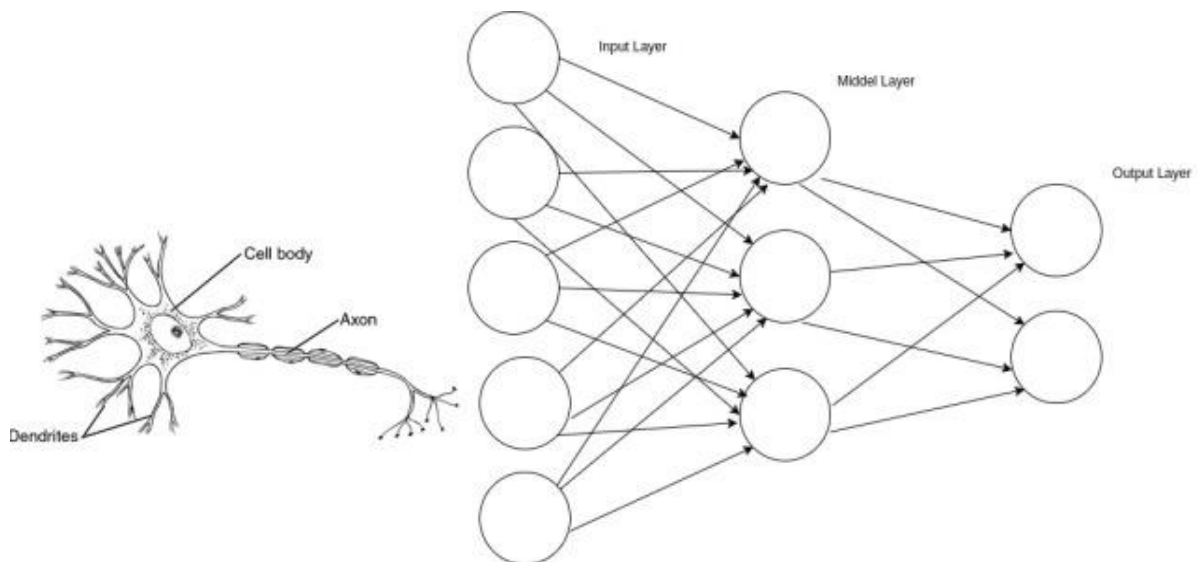


**Fig. 3.1** Comparison between biological neuron and an artificial neural network structure

### 3.2.1 Structure

The neuron is the fundamental computing unit of the neural network, it is formed by three basic elements of the neural model (figure 3.2) :

- A group of synapsis or connections, in which every of them is characterised by a weight (synaptic efficiency);
- An adder that sums the input signals that are weighted by respective synapsis, producing, as an output, a linear combination of the input;
- An activation function to limit the neuron output magnitude. Typically, for simplicity, the outputs magnitude belong to the interval  $[0,1]$  or  $[-1,1]$ .

The neuronal model include also a threshold value which has the effect to increase or to decrease the net input to the activation function [10].

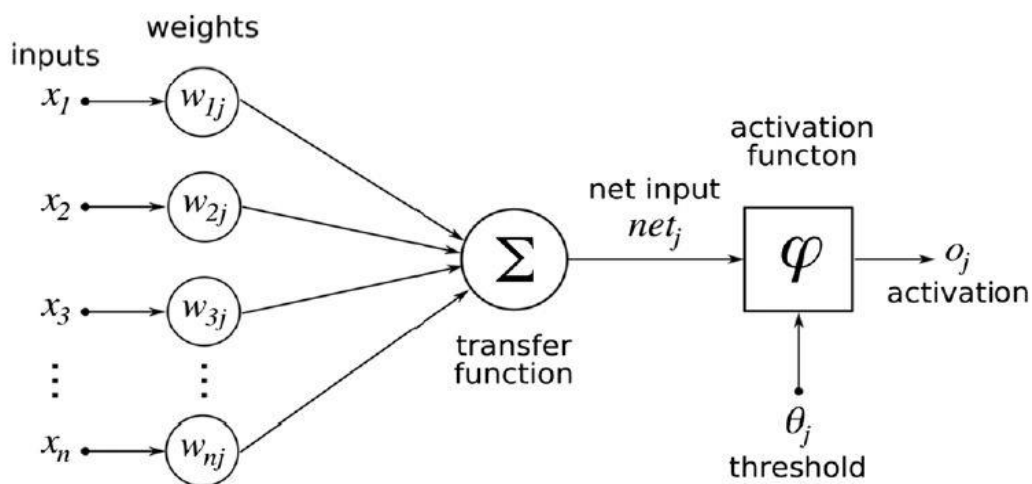


Fig. 3.2 Artificial neuron model

In mathematical terms it is possible to describe a neuron  $k$  through the following equations:

$$u_k = \sum_{j=1}^m w_{kj} \cdot x_j \quad (14)$$

$$y_k = \varphi(u_k + b_k) \quad (15)$$

Where:

- $w_{kj}$  are the synaptic weights of the neuron  $k$ ;
- $u_k$  is the linear combination of the input of the neuron  $k$ ;
- $b_k$  is the threshold value of the neuron  $k$ ;
- $\varphi$  is the activation function;
- $y_k$  is the output generated by the neuron  $k$ ;
- $m$  is the number of inputs.

### 3.2.2 Types of activation function

There are three different types of activation function:

- Threshold (or step) function (figure 3.3):

$$\varphi(x) = \begin{cases} 1, & x \geq 0 \\ 0, & x < 0 \end{cases} \quad (16)$$

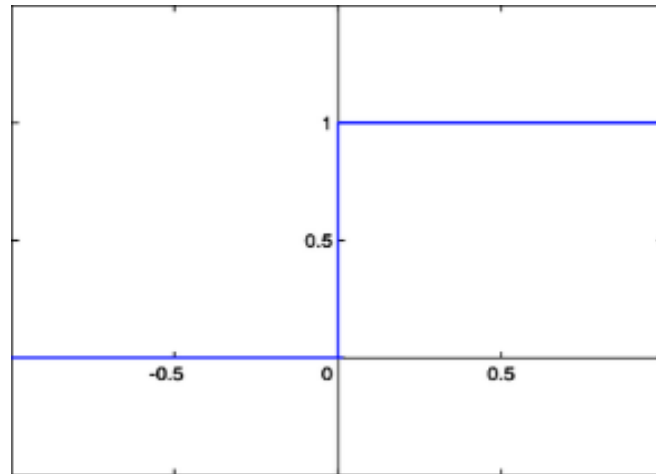


Fig. 3.3 Threshold function

- Linear function (figure 3.4):

$$\varphi(x) = x \quad (17)$$

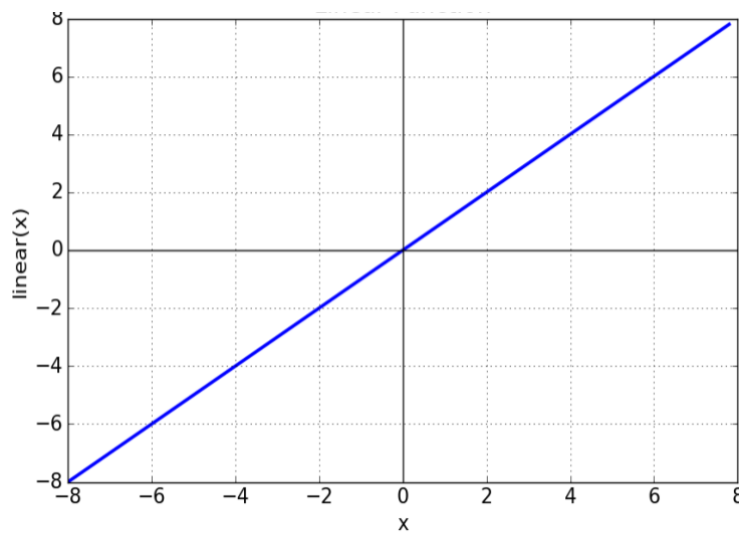


Fig. 3.4 Linear function

- Sigmoid function (figure 3.5):

It is the most used function in building up artificial neural network. It is a balance between the linear and the step function.

$$\varphi(x) = \frac{1}{1 + e^{-a \cdot x}} \quad (18)$$

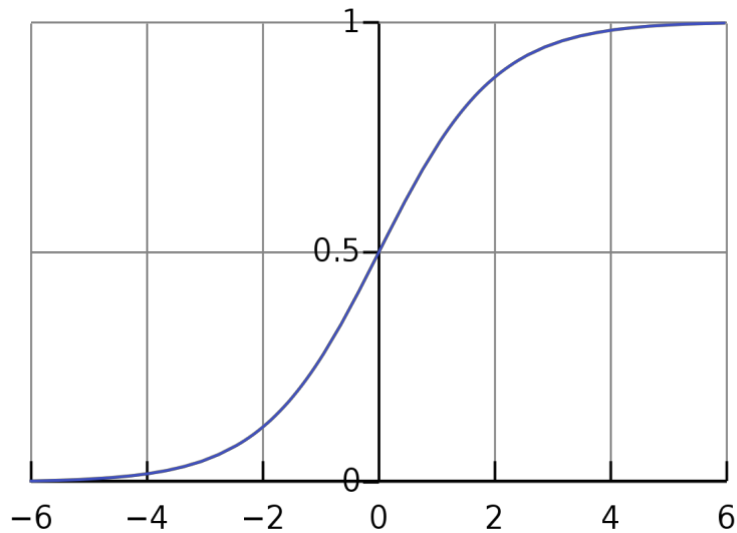


Fig. 3.5 Sigmoid function

Where  $a$  is a pendency parameter.

### 3.2.3 Neural network architectures

The type of neural network architecture depends on the learning algorithm and the application used. In general, there are three main architecture categories:

- One layer feed-forward (figure 3.6)

In this form, there is an input layer, a hidden layer and an output layer. The network signal is propagating forward, starting from the input layer and finishing in the output one.

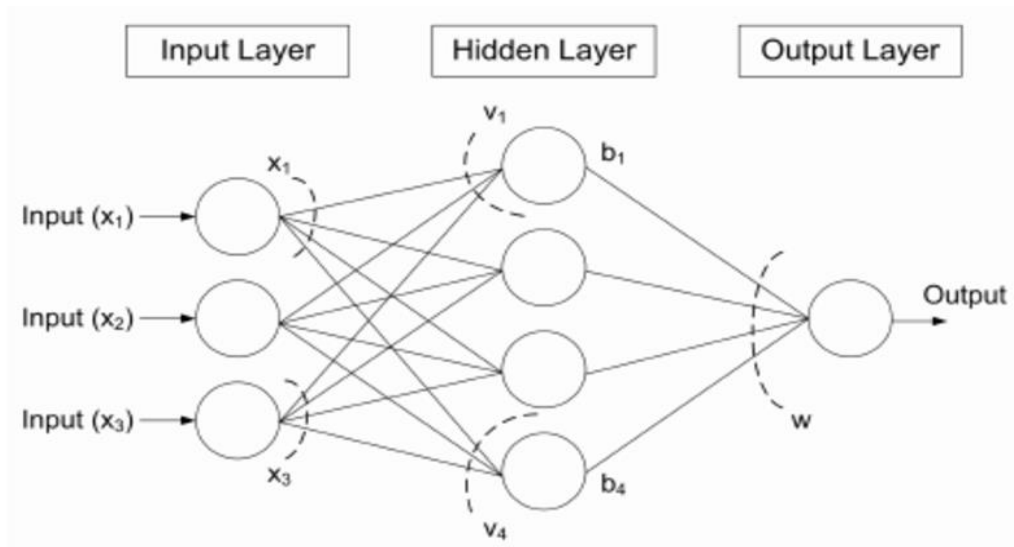


Fig. 3.6 One layer Neural network feed-forward

- Multi-layer feed-forward (figure 3.7)

This network category has additional layers between the input and the output layer (hidden layers). Each layer has input connection from the previous layer and output to the following layers, thus the propagation of the signal is forward without cycle or transversal connections.

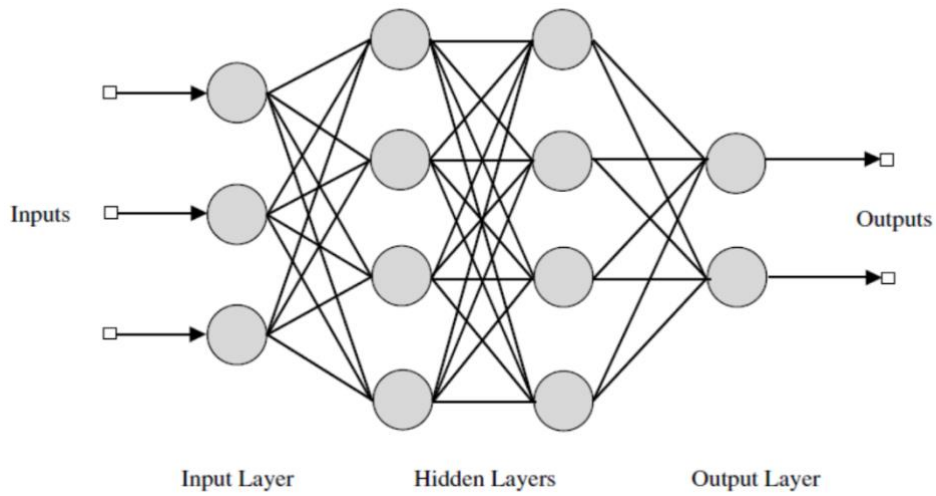


Fig. 3.7 Multi-layer Neural network feed-forward

- Recurrent feed-forward (figure 3.8)

A recurrent network is a cyclic network. The presence of cycles has a particular impact on the network learning capacity and on its performance.

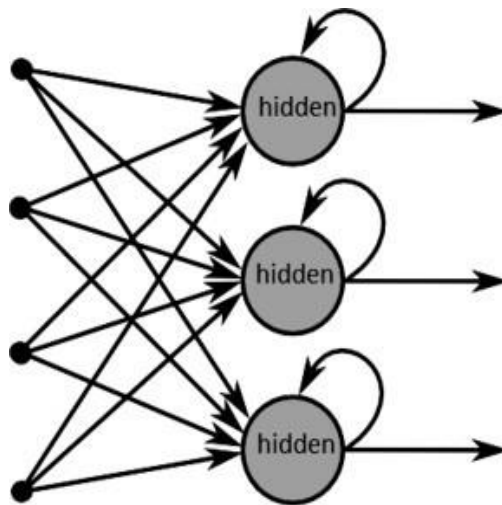


Fig. 3.8 Recurrent feed-forward network

### 3.2.4 Learning algorithms

The learning phase is a process in which free neural network parameters are adapted, through an iterative stimulation process. The type of learning is determined by how such adaptations occur.

A learning algorithm can be divided in two categories:

- *Supervised algorithm*, the correct correlations input/output are provided to the network; the network will fix its free parameters depending on the correlation provided.
- *Unsupervised algorithm*, the network learns independently.

Some of the most important learning algorithm are described below;

#### ALGORITHMS BASED ON ERROR CORRECTION

Each neuron  $k$  receives as input a stimulus signal  $x(n)$  and generates an output  $y_k(n)$ , with  $n$  discrete time.  $d_k(n)$  is the desired output. Consequently, it is generated an error signal  $e_k(n)$ .

$$e_k(n) = d_k(n) - y_k(n) \quad (19)$$

The error signal  $e_k(n)$  carries out a control mechanism in order to apply an adjustment sequence of the synaptic weight to accost the answer obtained  $y_k(n)$  and the desired  $d_k(n)$ .

This process occurs step by step minimizing a cost function:

$$E(n) = \frac{1}{2} \cdot e_n^2(n) \quad (20)$$

To do so the gradient method or Widrow-Hoff method are used. Supposing  $w_{kj}(n)$  is the synaptic weights of the neuron  $k$  stimulated by the element  $x_j(n)$ , then the adjustment to  $w_{kj}(n)$  is:

$$\Delta w_{kj}(n) = \eta \cdot e_k(n) \cdot x_j(n) \quad (21)$$

Where  $\eta$  is called *learning rate*.

The new weights will be:

$$w_{kj}(n+1) = w_{kj}(n) + \Delta w_{kj}(n) \quad (22)$$

The backpropagation algorithm is an example of a system in which the stability depends on parameters and in particular on  $\eta$ . The choice of this parameter is important as it affects the convergence and stability of the learning process.

#### ALGORITHM BASED ON MEMORY

In this kind of algorithm, all (or the majority) of the past experiences are recorded in a large memory of input-output couples correctly classified  $\{(x_i, d_i)\}_{i=1}^n$ , where  $x_i$  is the input vector and  $d_i$  is the desired output. When the classification of an example not known  $x_{test}$  is required, the system reacts

## CHAPTER 3. DATA MINING

finding and analysing the examples in memory that are in a  $x_{test}$  neighbourhood.

All the method based on memory involves 2 main concepts:

- Criteria used to define the neighbourhood of  $x_{test}$
- Learning approach applied to the neighbourhood of  $x_{test}$

An example is the k-nearest neighbourhood in which:

- The neighbourhood of the test example is the group of  $k$  examples memorised closest to the test example;
- The class assigned is the one with the high frequency in the neighbourhood of the example test.

## COMPETITIVE LEARNING

With the competitive learning the output neurons of a neural network compete between them in order to become activated. Only one neuron can be activated in a certain time  $n$ .

There are three basic elements regarding the competitive learning:

- A set of equal neurons with synaptic weights generated randomly that reacts in different way to given input data;
- A limit to the “force” of each neuron;

- A mechanism that enables the neurons to compete to have the right to react to a given input subset in order to have only one neuron group activated per time.

In this way the neurons tend to specialize on a set of similar inputs [11].

### 3.2.5 Single layer and Multi layer perceptron

The perceptron is the simplest neural network structure, it is used to classify pattern separable linearly, or rather pattern that are in opposite sides on a hyperplane.

It consists of a single neuron with synaptic weight and threshold modifiable (figure 3.9).

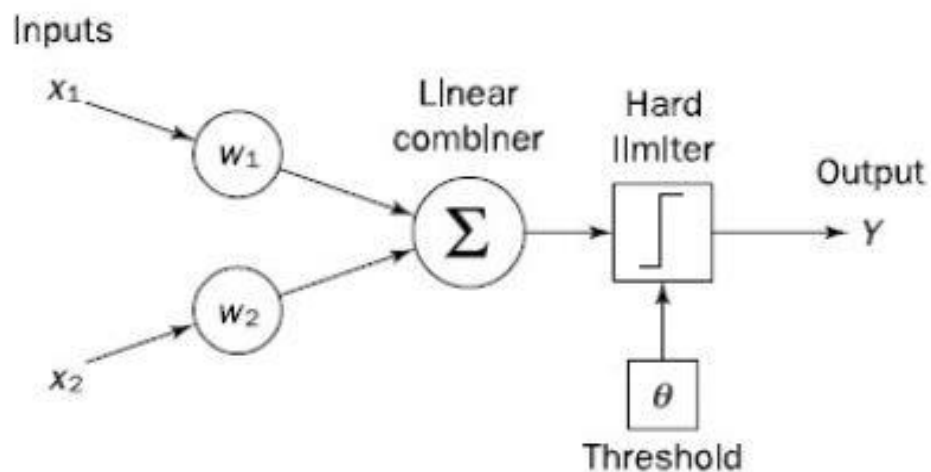
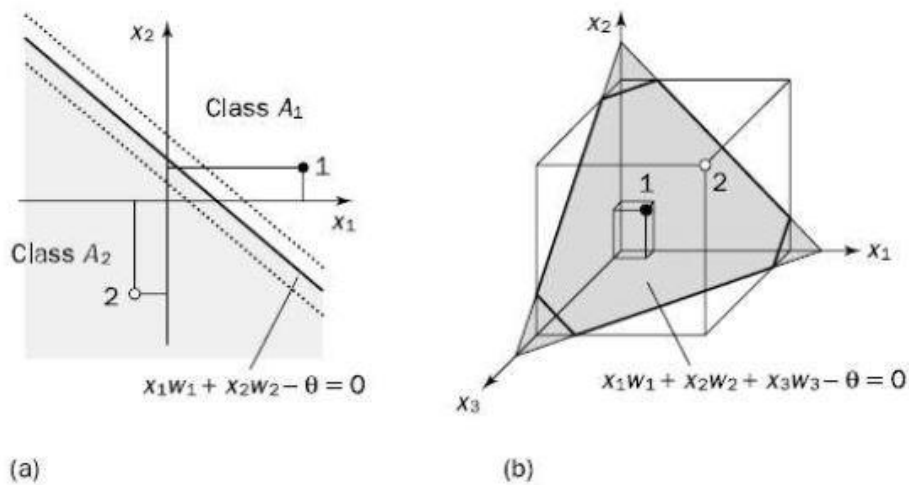


Fig. 3.9 Schematic of a perceptron

Frank Rosenblatt proved that if the chosen patterns to train the network belongs to two class that are linearly separable, thus the learning algorithm converges and the decisional space is divided in two parts by an hyperplane (figure 3.10). This theorem is called the perceptron convergence theorem.



**Fig. 3.10** Linear separability in perceptrons: (a) two-input perceptron; (b) three-input perceptron

Multilayer perceptron (MLP) (figure 3.11) consists of an input layer, one or more hidden layers and an output layer. The signal propagates forward layer by layer.

MLPs with one hidden layer are capable of approximating any continuous function, furthermore are usually applied to supervised learning approach: they train on a set of input-output pairs and learn to model the correlation between those inputs and outputs. Training enhances to adjust the weights and biases of the model in order to minimize error between the output and

the target of that element. Backpropagation is used to make those weights and bias adjustments relative to the error.

Feed-forward networks such as MLPs has two different type of motions, a constant back and forth.

In the *forward pass*, the signal flow moves from the input layer to the output layer, and the decision of the output layer is measured against the ground truth labels.

In the *backward pass*, using backpropagation and the chain rule of calculus, partial derivatives of the error function w.r.t. the various weights and biases are back-propagated through the MLP. That act of differentiation gives a gradient, or a landscape of error, along which the parameters may be adjusted as they move the MLP one step closer to the error minimum. This can be done with any gradient-based optimisation algorithm, such as stochastic gradient descent. The network iterating until the error is below a specified threshold. This state is known as *convergence*.

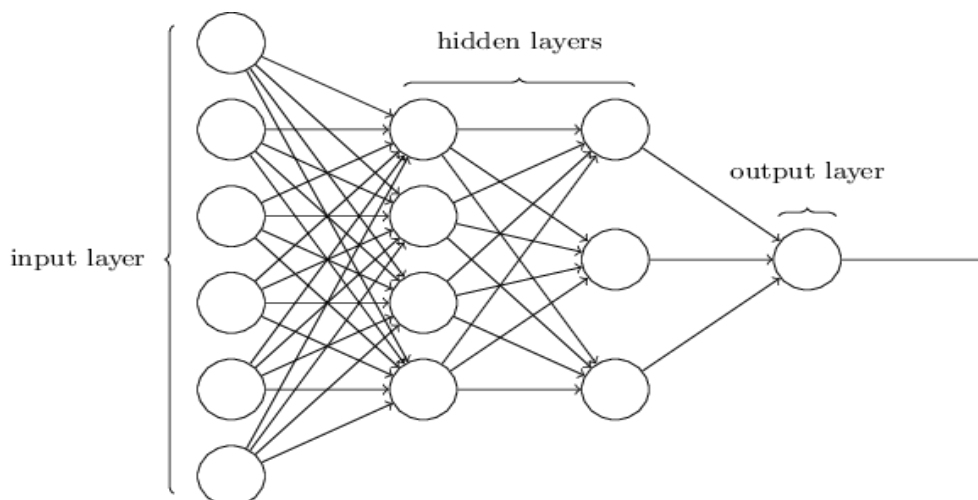


**Fig. 3.11** Schematic of Multilayer perceptron

### *3.2.6 Feature extraction*

Regarding Data mining, a feature is a measurable property of a phenomenon being observed. Choosing discriminating and independent features is key to any pattern recognition algorithm being successful in classification.

Feature Extraction aims to identify the important characteristics or features representing the context of interest (for example a particular pathology, motion or state of the body).

Features can be extracted in different ways:

- directly from measurements or experts' judgments
- applying different processing techniques to a set of acquired signals, measurements or images.

In this study the following features have been extracted:

- Normalization of the acceleration between the maximum and the minimum of the function;
- Normalization of the gyroscope between the maximum and the minimum of the function;
- Differentiation of the acceleration;
- integration of the acceleration (velocity);
- double integration of the acceleration (displacement);
- Stance phase.

All of these features were extracted per each stride.

### 3.3 State of the art

Several studies were accomplished to define 3D GRF using force platforms, pressure matrix or sensors in combination with ANN.

Recent studies in the Swinburne University of Technology (Hawtorne, Melbourne, Australia) have investigated the ability of wearable sensors in combination with artificial neural network (ANN) and multiple linear regression (MLR) models, for the estimation of GRF during running phase. It has been developed a particular data acquisition system in order to obtain in-shoe force (ISF) data (figure 3.12); afterwards, the correlation between the data from wearable sensors (source data) and force platform (target data) was obtained.

In prediction terms, the MLR model was discovered to provide an high level of precision for the prediction of the vertical and medium-lateral components of GRF and the ANN model provided the most accurate predictions of the anterior-posterior component of GRF. In this particular study, the wearable sensors were composed by matrix pressure in-shoe system; four discrete hydrocell in-shoe force (ISF) sensors were disposed to the left foot-shoe interface of the subject at the heel, first and third metatarsal head and hallux, given that these positions correspond to the major anatomical load bearing structures of the foot in running (Henning and Milani, 1995) [12].

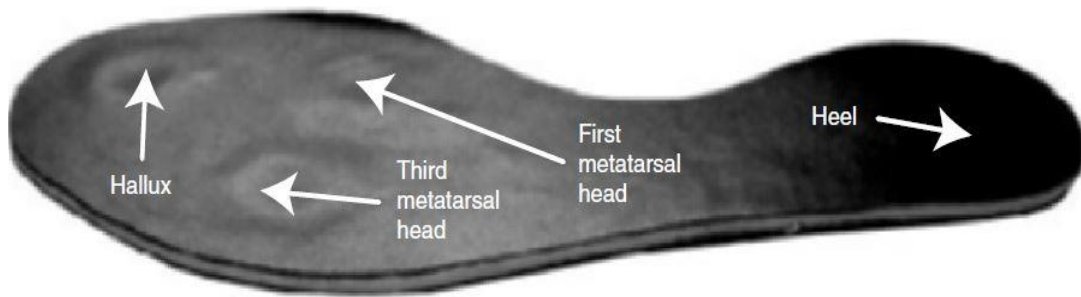


**Fig. 3.12** Complete insole detailing sensor locations

Another recent study has led to the realization of two different artificial neural networks (one network with three outputs and three networks with one output each) based on accelerometer data, in order to analyse and compare the residuals obtained from ground reaction force (GRF) models; specifically, seventeen healthy subjects walked along a walkway, with an embedded force plate, with a tri-axis accelerometer fixed to the shank: Multilayer perceptron networks (MLP) models were performed in combination with the 3D accelerometer data as inputs to predict the GRF. The final results showed that there was no difference between the two network configurations (one network with three outputs (figure 3.13) and three networks with one output each) [13].

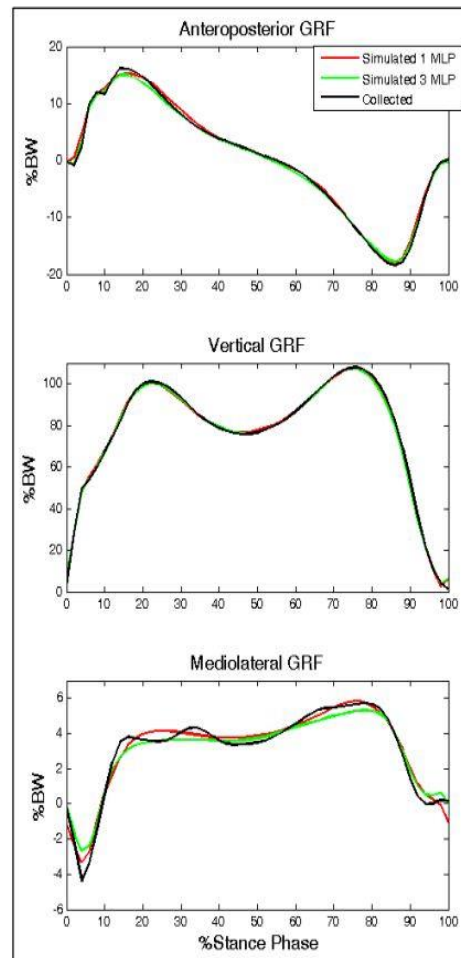


**Fig. 3.13** Collected and simulated GRF in both configurations

In an analogous study, Leporace used a feed-forward neural network in order to predict the ground reaction forces signals based on accelerometer during gait; another important study that is correlated with the main focus of the current thesis is the analysis performed by Frank J. Wouda about the “Estimation of Vertical Ground Reaction Forces and Sagittal Knee Kinematics during Running Using Three Inertial Sensors”; this study consisted to train two concatenated artificial neural networks:

- the first artificial neural network maps the information (orientation and acceleration) of three inertial sensors (placed at the pelvis and lower legs) to lower-body joint angles.
- the estimated joint angles in conjunction with measured vertical accelerations are input to a second artificial neural network that estimates vertical ground reaction forces.

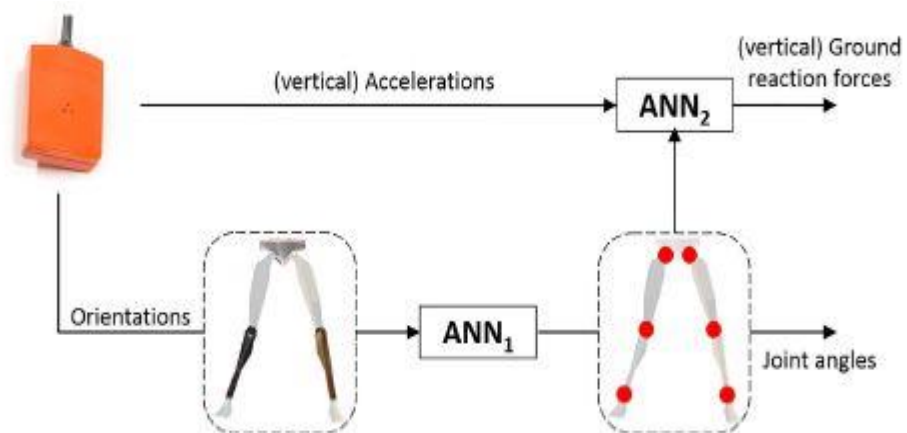


Fig. 3.14 Schematic of the system with the two concatenated ANN

This work has shown the power of estimating kinetics during running using a minimum number of on-body sensors (three sensors placed on the pelvis and lower legs) [14].

In another study, some researchers of the Chinese Culture University have used an artificial neural network with ground reaction forces as input, to estimate the joint torque of the lower limb; they used a fully-connected, feed forward network with one input layer, one hidden layer and one output layer trained by the back propagation algorithm. The input parameters of ANN

were relevant time variables (features selection) of GRF measurement and the output parameters were joint torque.

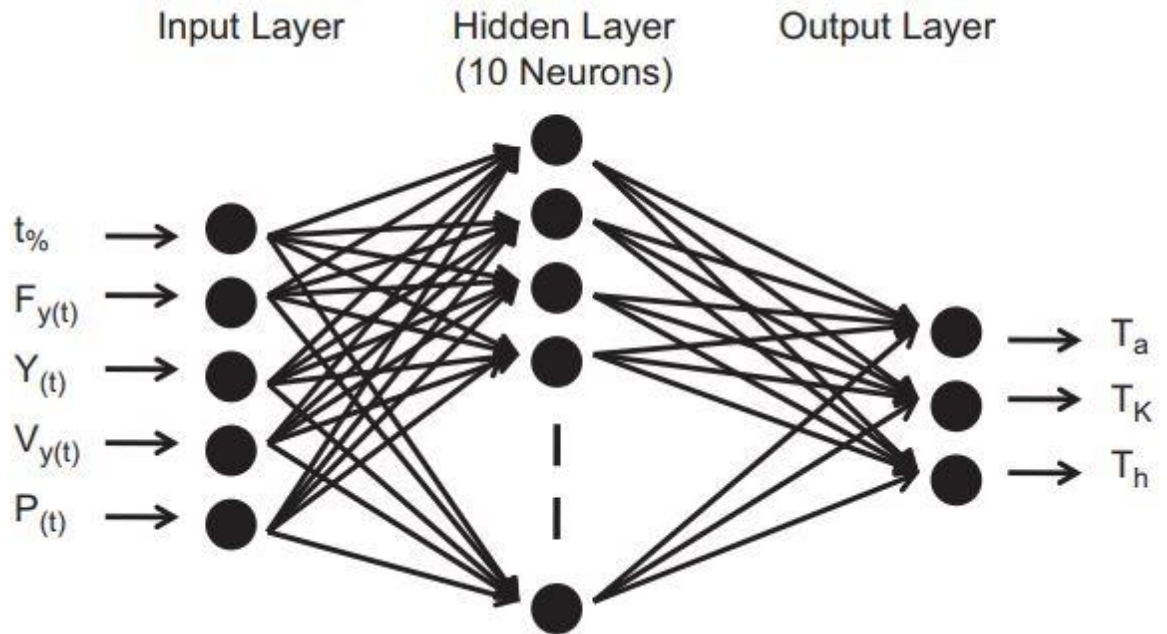


Fig. 3.15 Ann model that represents one of the best mapping tool for kinematic data

The final results have indicated that the ANN model developed in this study is feasible in the assessment of joint torque without inverse dynamic calculation [15].

# Chapter 4

## Data collection

In this chapter, the protocol used for the in-lab validation and the algorithm implemented to simulate the force platform waveforms are described.

### 4.1 Data acquisition

From the literature review ,it emerged that the use of inertial sensor is a good option for estimating GRF. In general, GRF can be predicted from IMU data by using a biomechanical model in conjunction with Newton's second law of motion, or a machine learning approach.

The most critical aspects in determining GRF using machine learning were found to be:

- The number of sensors/body segments required for the data acquisition;

- Determining the antero-posterior and medio-lateral components of GRF.

Increasing the number of sensors means having a better knowledge of motion and acceleration of each body part, leading to a more accurate estimation of GRF. On the other hand, reducing the number of sensors would dramatically simplify subject preparation, data acquisition and subject's comfort.

As a tool to collect data, the “Actigraph GT9X” has been considered.

The ActiGraph GT9X (figure 4.1) captures and records high resolution raw data: an integrated IMU containing a 3D gyroscope (2000°/sec), 3D magnetometer, and a 3D accelerometer (16g) sensors which provides raw position and rotational data for a variety of advanced applications, including running analysis. The sampling frequency is 100 Hz, which is sufficient for the purpose of this study.



**Fig. 4.1** Actigraph GT9X

## CHAPTER 4. DATA COLLECTION

The study is based on one cohort: a sample of 10 healthy young adults (7 males, age:  $27 \pm 4$ , weight:  $82.14 \text{ kg} \pm 19$ , height:  $1.80\text{m} \pm 0.15$ , 3 females).

Volunteers were recruited via a general invitation e-mail, posters, and word of mouth, to staff, ex-staff, and students at the University College Cork.

The inclusion criteria were age between 23 and 35, with no history of neurological or other disorders or disability that could affect subject's movements, in good general health, and not pregnant.

During the trials, the subjects wore two Actigraphs on the shanks (figure 4.2).



**Fig. 4.2** Actigraphs wore on the shanks

The protocol adopted was performed as follows:

- Running on a treadmill at 8 km/h for the first 60 seconds;
- Running at 10 km/h for the following 60 seconds;
- Running at 12 km/h for the following 60 seconds;

The neural network established the relation between the Actigraph raw data and the vertical ground reaction forces correlated reproduced by an algorithm (Clark's method) described afterwards.



**Fig. 4.3** Running on the treadmill during trials

## 4.2 GRF waveform reproduction

It has been necessary to find a solution to reproduce realistic Ground Reaction Forces from the subjects, as an instrumented treadmill or a suitable force platform was not available during this study.

Clark's method [16] consists of a theoretical model that states that the force contributions of two discrete body mass components are sufficient to account for vertical ground reaction forces during running phase. More in details, this method is based on the concept that humans during running have a general complexity due to limb-segment morphology, neural control of muscle forces and tissue properties. All of these features enhances the different body masses to accelerate differently with respect to one another and the ground. The waveform related to the ground reaction force corresponds to the total acceleration of the different body's masses, then the sum of the acceleration of the different masses must yield the waveform patterns.

This approach divides the body main masses into two (figure 4.4):

- $m_1$  that corresponds to the mass of the lower limb (8% of the total body mass);
- $m_2$  that correspond to the rest of the body's mass (92% of the total body mass).

Thus, there are two different forces (impulses) that contribute to the vertical force waveform:

- Impulse  $J_1$ , yielded from the vertical collision of  $m_1$  with the running way;
- Impulse  $J_2$ , yielded from the vertical accelerations of  $m_2$  throughout the ground contact period.

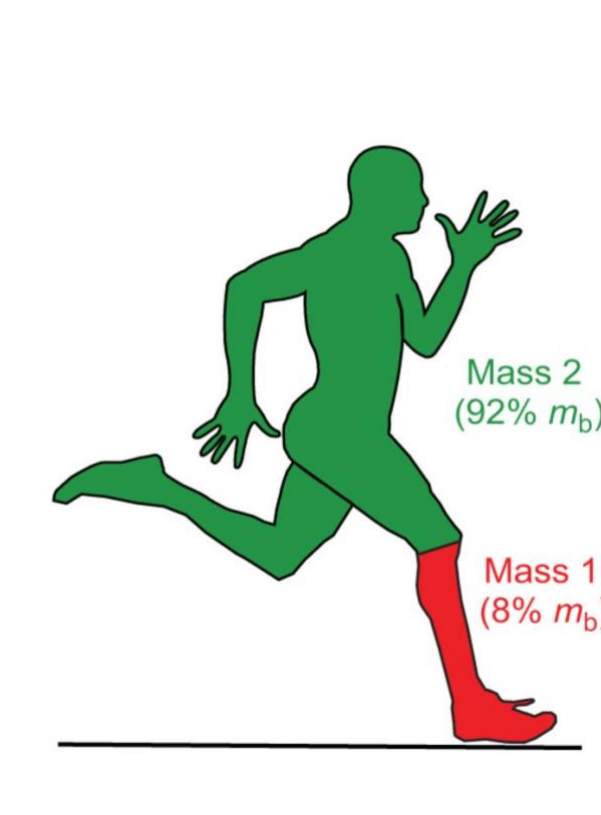


Fig. 4.4 Two mass-model

The model implemented needs as inputs only the body mass of the subject and three specific measures: contact time, flight time and lower limb acceleration.

## CHAPTER 4. DATA COLLECTION

The total vertical ground reaction force is composed of two overlapped impulses mentioned before ( $J_1$  and  $J_2$ ); the total ground reaction impulse  $J_T$  during the ground contact time ( $F_{T,avg}t_c$ ) is:

$$J_T = J_1 + J_2 = F_{T,avg}t_c \quad (23)$$

The model assumes that speed is constant during running; the averaged vertical ground reaction forces must be equal to the body's weight, and  $F_{T,avg}t_c$  is equal to:

$$F_{T,avg} = m_b g \frac{t_c + t_f}{t_c} \quad (24)$$

Where:

- $m_b$  is the body mass;
- $g$  is the gravity acceleration;
- $t_c$  is the contact time;
- $t_f$  is the flight time;
- $t_c + t_f$  is the step time  $t_{step}$ .

Impulse  $J_1$  corresponds to the vertical deceleration of  $m_1$  during the impact with the surface:

$$J_1 = F_{1,avg}(2\Delta t_1) = (m_1 \frac{\Delta v_1}{\Delta t_1} + m_1 g)(2\Delta t_1) \quad (25)$$

Where:

- $\Delta t_1$  is the interval of time between touchdown and the vertical speed of  $m_1$  decreasing to zero;
- $\Delta v_1$  is the change in vertical velocity of  $m_1$  during  $\Delta t_1$ ;
- $F_{1,avg}$  is the average force of impulse  $J_1$ ;

Impulse  $J_2$  corresponds to the rest of the body's mass and it is equal to:

$$J_2 = F_{2,avg}t_c = J_T - J_1 \quad (26)$$

Where  $F_{2,avg}$  is the average force of impulse  $J_2$  during the contact time  $t_c$ .

The raise cosine bell (RCB) function has been used to generate the bell shaped force curve  $F(t)$  of  $J_1$  and  $J_2$ .

The raised cosine function can be obtained from the first two terms of the Fouries series:

$$F(t) = a_0 + \sum_{N=1}^N a_n \sin(2\pi f_n t + \theta_n) \quad (27)$$

Where  $a_0$  is the average of the signal, and  $a_n$ ,  $f_n$  and  $\theta_n$  are the amplitude, frequency and phase angle of the  $n$ th harmonic.

The first two terms of the Fourier series are:

$$F(t) = a_0 + a_1 \sin(2\pi f_1 t + \theta_1) \quad (28)$$

## CHAPTER 4. DATA COLLECTION

Hence, it results equivalent to:

$$F(t) = a_0 + a_1 \cos(2\pi f_1 t) \quad (29)$$

Term  $a_0$  is the average of the function, and term  $a_1$  is the amplitude of the function. Each term is defined by the total peak amplitude  $A$ , resulting in  $a_0 = a_1 = A/2$ . The peak is situated at center time  $B$ .

Frequency  $f_1$  can be defined in terms of width parameter  $C$ , which is defined from the peak at  $t=B$  to the time where  $F(t)$  decays to zero, resulting in  $f_1 = 1/(2C)$ . The constants  $A$ ,  $B$  and  $C$  are inserted into Equation 29 to determine the raised cosine periodic function:

$$F(t) = \frac{A}{2} + \frac{A}{2} \cos\left(\frac{\pi}{C}(t - B)\right) \quad (30)$$

The force waveform  $F_1(t)$  of the impulse  $J_1$  is equal to:

$$F_1(t) = \frac{A_1}{2} \left[ 1 + \cos\left(\frac{t - B_1}{C_1} \pi\right) \right] \quad (31)$$

Where:

- $A_1 = 2F_{1,avg}$  using  $F_{1,avg}$  of the equation 25
- $B_1$  and  $C_1$  are equal to the time  $\Delta t_1$  after touchdown for the vertical velocity of  $m_1$  to reach zero.

The force waveform  $F_2(t)$  of the impulse  $J_2$  is equal to:

$$F_2(t) = \frac{A_2}{2} \left[ 1 + \cos\left(\frac{t - B_2}{C_2} \pi\right) \right] \quad (32)$$

Where:

- $A_2 = 2F_{2,avg}$  using  $F_{2,avg}$  of the equation 25
- $B_1$  and  $C_1$  are equal to the time  $\Delta t_1$  after touchdown for the vertical velocity of  $m_1$  to reach zero.

The two force waveform contributions yield:

$$F_T(t) = F_1(t) + F_2(t) \quad (33)$$

The temporal position of the peak of impulse  $J_2$  depends on the relative position of the centre of mass at touchdown and take off. An ideal spring-mass running has symmetrical centre of mass of displacement, consequently the profile is symmetrical where the location of the peak  $B_2$  is  $0.5t_c$ . Nevertheless, the stance leg is more extended at take off than at touchdown, and this yield an higher mass centre at take off than the one at touchdown, which results in an asymmetrical impulse  $J_2$  profile.

It is possible to include width parameters to control the symmetry of the waveform  $F_2(t)$ :

$$F_2(t) = \begin{cases} 0 & t < B_2 - C_{2L} \\ \frac{A_2}{2} \left[ 1 + \cos \left( \frac{t - B_2}{C_{2L}} \pi \right) \right] & B_2 - C_{2L} \leq t \leq B_2 \\ \frac{A_2}{2} \left[ 1 + \cos \left( \frac{t - B_2}{C_{2T}} \pi \right) \right] & B_2 < t < B_2 + C_{2T} \\ 0 & t > B_2 + C_{2T} \end{cases} \quad (34)$$

Where  $A_2$  is the peak amplitude,  $B_2$  is the centre time of the peak,  $C_{2L}$  is the leading half-width time interval, and  $C_{2T}$  is the trailing half-width time interval. The location of peak  $B_2$  has been settled at  $0.47t_c$ .

Figure 4.5 represents an illustration of mass segment  $m_1$  motion during the foot-ground portion of a running step, the red circle represents the axis of rotation of the ankle joint:

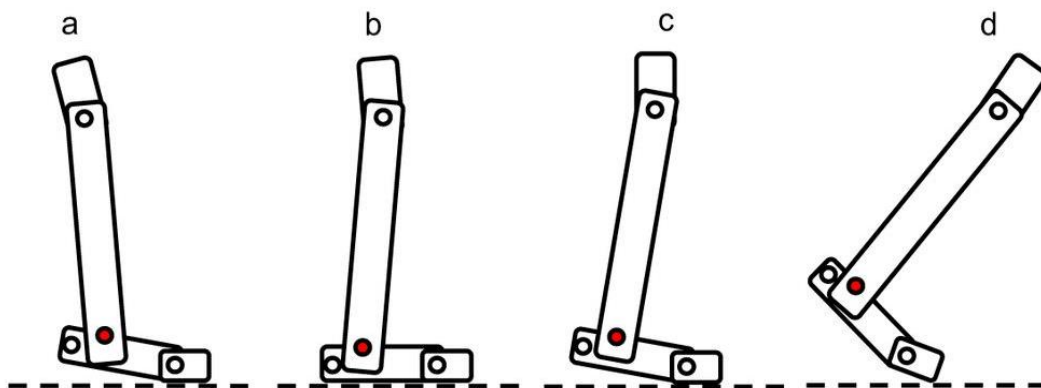
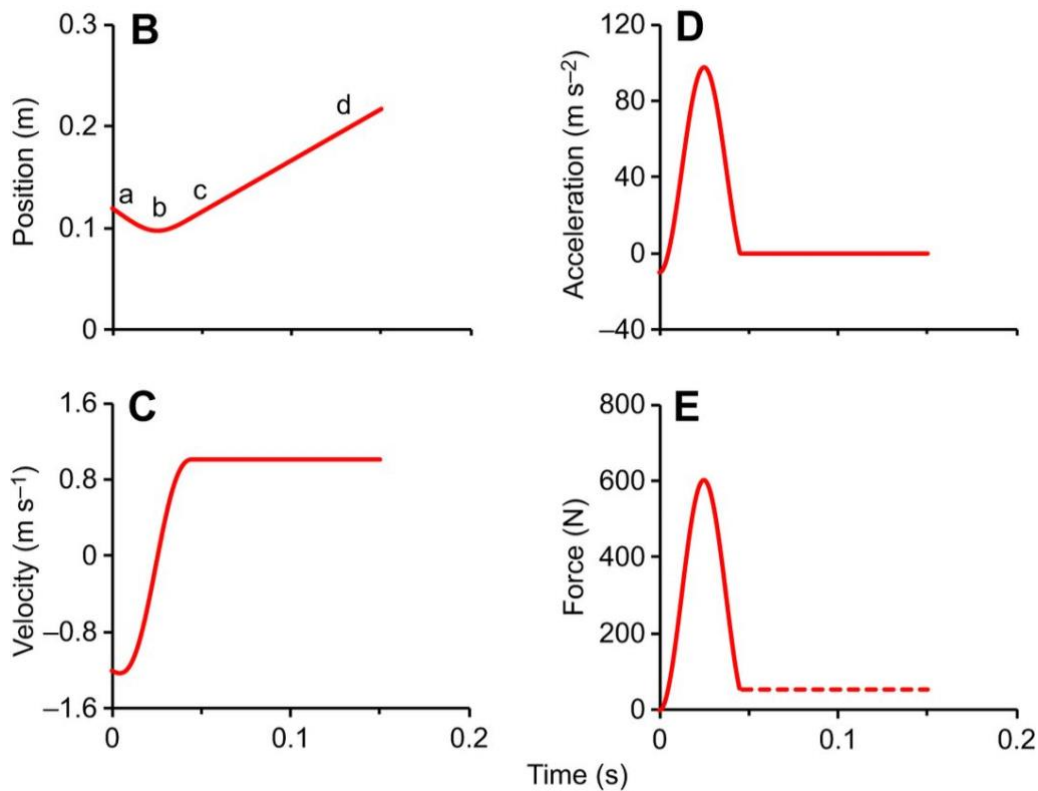


Fig. 4.5 Lower limb motions



**Fig. 4.6** Different schematic graphs for vertical position (B), velocity (C), acceleration (D), and force (E) of the lower limb mass  $m_1$

Figure 4.6 shows how after the impact interval,  $m_1$  reaches a relatively constant positive speed, ensuing in near-zero acceleration of  $m_1$ . A simplifying assumption of the two-mass model allows to model the force resulting from the acceleration of  $m_1$  into a finite impulse during the impact period.

This method provides the representation of the GRFs when using marker-based devices, such as the optoelectronic system.

Figure 4.7 illustrates an example of GRF waveform recreated via re-adopting the Clark's method via motion sensors:

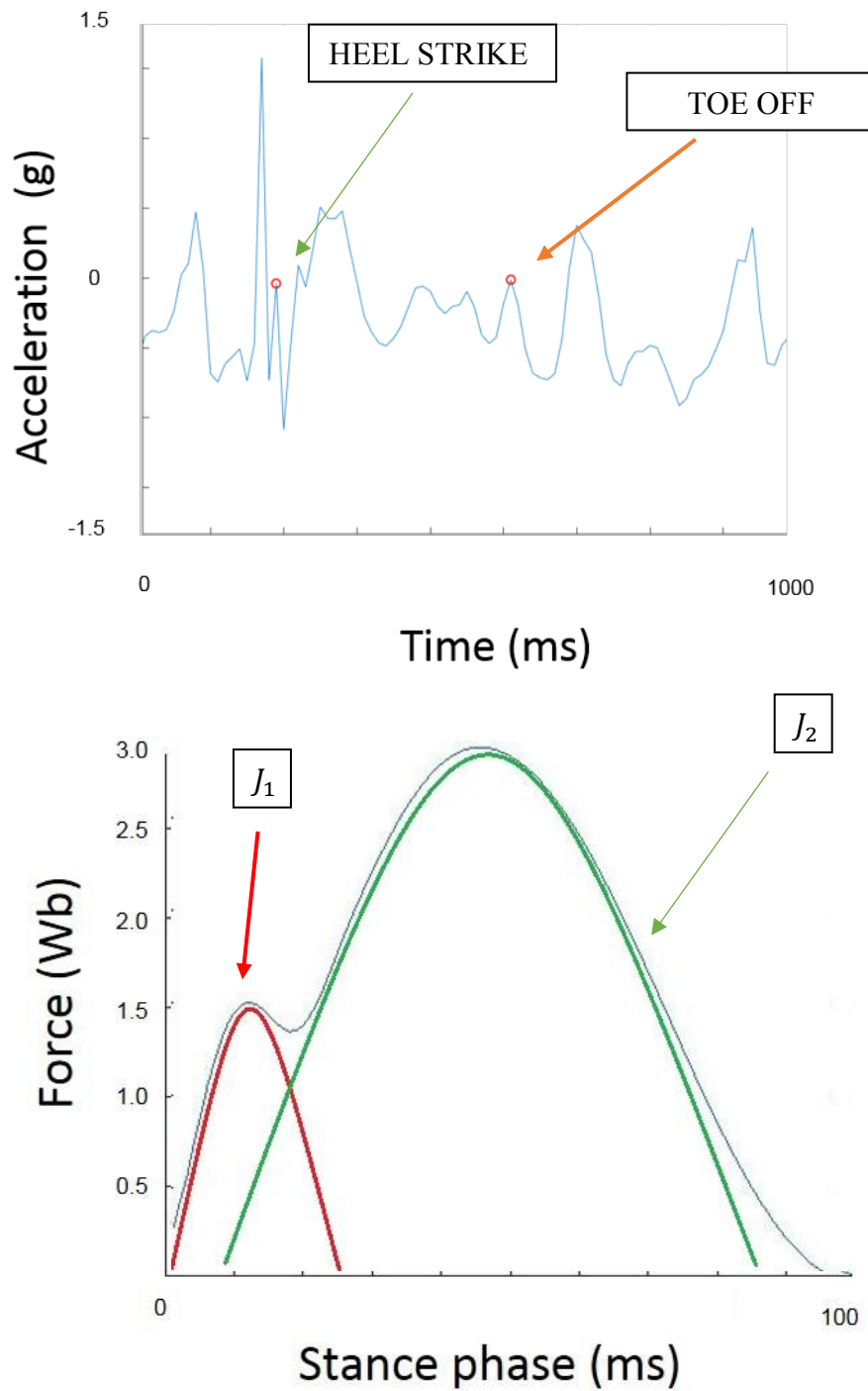


Fig. 4.7 GRF recreated via Clark's method from motion sensors

# Chapter 5

## Results

In this chapter, the algorithm implemented to define and validate the ANN algorithm to predict the GRFs, will be described.

Consequently, results obtained in terms of Mean Absolute Error (MAE) and Pearson correlation coefficient ( $R$ ) will be discussed.

### 5.1 Learning approach

The proposed learning approach relies on data from the two actigraph sensors (placed at lower legs), which fed the ANN. The artificial network maps different features (described in 3.2.6) of inertial data to vertical ground reaction forces.

Several ANN were trained using 16 inputs, namely the number of the features, and different number of neurons in one single hidden layer (from 5

neurons to 100 neurons) were adopted. The output layer consisted of only one neuron. The activation function used in the neurons of the hidden layer was a sigmoid function.

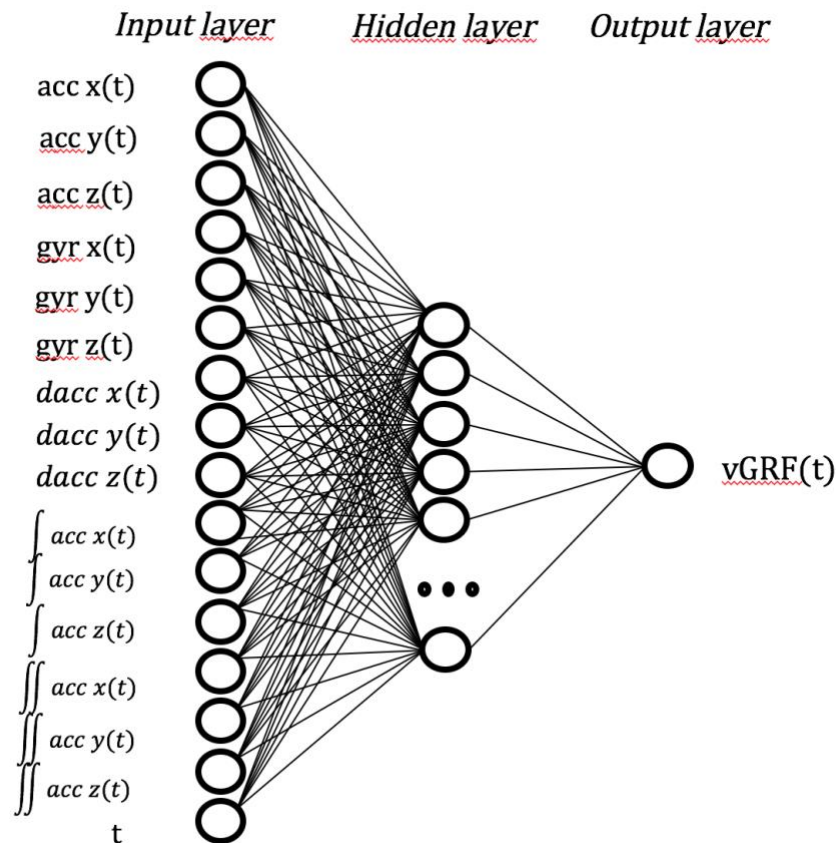


Fig. 5.1 Graph of the networks realized

The networks were trained for 2,000 iterations and training was stopped early if the gradient did not decrease for 6 consecutive iterations or if the gradient was smaller than  $1 \times 10^{-6}$ . The neural network toolbox of MATLAB R2016b (Mathworks, Inc., Natick, MA, USA) was used to design, train, and evaluate the ANNs described above.

In this study, it has been used a Leave One Subject Out - Cross Validation (LOSO – CV) approach: it has been divided the dataset in  $n$  partition that corresponds to the  $n$  subjects. Two partitions were removed temporary from the dataset, for the final testing of the system; in the remainder development dataset, one partition was considered as the validation set, while the remaining ones were as training set.

This procedure is repeated  $k$  times; every time a different folder is chosen for the validation, in order to obtain  $k$  estimation of the test error.

The cross validation then computes the average error for the  $k$  folders.

To define the most performant topology of neural networks, the LOSO - CV has been repeated for several topologies with different neurons in the hidden layer (5 neurons until 100 neurons).

Finally, the chosen topology was used to calculate the final performance using the full dataset, which includes also the two subjects initially removed.

## 5.2 Outcome measures

The Mean Absolute Error (MAE) was adopted to estimate the prediction error of the ANN:

$$MAE = \frac{\sum_{i=1}^n |y_i - x_i|}{n} = \frac{\sum_{i=1}^n |e_i|}{n} \quad (35)$$

## CHAPTER 5. TEST AND VALIDATION

Where:

- $y$  is the true value, namely the GRFs that has to be predicted;
- $x$  is the value predicted, namely the several GRFs predicted by ANN;
- $n$  is the number of samples that compose the signal.

The Mean Absolute Percentage Error (MAPE) was adopted for the prediction of the error of the most performant ANN topology; it is an extension of the MAE:

$$MAE = \frac{100\%}{n} \sum_{i=1}^n \left| \frac{y_i - x_i}{y_i} \right| \quad (36)$$

The Pearson correlation coefficient ( $R$ ) is an index that finds a possible linear relationship between two statistical variables; given two variables  $X$  and  $Y$  ( $X$  is the GRF predicted and  $Y$  the one that has to be predicted),  $R$  is defined as:

$$R = \frac{\sigma_{XY}}{\sigma_X \sigma_Y} \quad (37)$$

Where:

- $\sigma_{XY}$  is the covariance between  $X$  and  $Y$ ;
- $\sigma_X$  and  $\sigma_Y$  are the two standard deviations.

$R$  can assume values between -1 and 1:

- If  $R > 0$ , the X and Y variables are positively correlated;
- If  $R = 0$ , the X and Y variables are uncorrelated;
- If  $R < 0$ , the X and Y variables are negatively correlated.
- If  $R = 1$ , the X and Y variable are totally correlated.

MAE and R have been computed for every single partition; afterwards, they have been averaged.

The topology that yield the lower MAE and the higher R, has been chosen for the final test on the two partitions removed previously.

### 5.3 Results

Figure 5.1 shows MAE and R for the different topologies:

		NUMBER OF NEURONS IN THE HIDDEN LAYER								
		5	10	15	20	25	30	35	40	100
MAE (N/KG)		0.52 ±	0.52 ±	0.53 ±	0.51 ±	0.50 ±	0.48 ±	0.49 ±	0.48 ±	0.47 ±
		0.16	0.14	0.14	0.14	0.14	0.14	0.14	0.14	0.17
R		0.91 ±	0.92 ±	0.92 ±	0.92 ±	0.92 ±	0.93 ±	0.92 ±	0.93 ±	0.92 ±
		0.07	0.06	0.06	0.05	0.05	0.05	0.05	0.05	0.06

**Fig. 5.2** Table with MAE and R for the different ANN topologies

In general, all the networks present comparable values of MAE, and high correlation.

## CHAPTER 5. TEST AND VALIDATION

It is possible to notice that the network with 30 neurons in the hidden layer, presents the best compromise between MAE, R and computational effort as it contains lower number of neurons.

Consequently, the network with 30 neurons in the hidden layer has been tested with two partitions that were temporary removed previously.

Figure 5.2 shows MAE, MAPE and R for the most performant network topology, furthermore it is listed also the error of the peaks (E of max) between the target and the predicted curves, the error of the means (E of mean) between target and prediction, and also MAPE.

MAE (N/Kg)	$0.49 \pm 0.15$
MAPE (%)	$0.13 \pm 0.04$
R	$0.91 \pm 0.13$
Peak Estimation Error (N/Kg)	$0.49 \pm 0.3$
Peak Estimation Error (%)	8.62
Mean Estimation Error (N/Kg)	$0.24 \pm 0.19$
Mean Estimation Error (%)	8.57

**Fig. 5.3** Table with MAE and R of the network with 30 neurons in the final testing

### 5.3.1 Discussion

The results show that the selected network has a limited MAPE value and this confirms the good performance of the network with 30 neurons, as it is able to predict the vGRFs with a restrained error value.

Furthermore, it is worth highlighting that the Peak Estimation Error and the Mean Estimation Error; both cases are lower than 10%. This means that it is possible to estimate the peaks properly, in order to measure the maximal work which the athletes are submitted during sports movements, and likewise it is possible to give correct estimations of the average workload of the athletes.

Finally, the R results confirm the good performance of the network in the linear correlation between the curve target and the curve estimated.

## 5.4 Future works

Summarising, method able to estimate vGRFs and relative key parameters based on ANNs in combination with motion sensors, has been developed.

As regards the error estimation of the vGRFs, it has been noticed how the algorithm has a good accuracy, but this performance could be yet improved.

This is because the target curve adopted, are simulated according to

## *CHAPTER 5. TEST AND VALIDATION*

biomechanical models and thus it is important to understand how performance change when using real-world GRFs.

Furthermore, in the present thesis it have been tested with only one hidden layer, but it is important to evaluate topologies varying also the number of hidden layer and the activation function, or adopting a deep learning approach.

Lastly, it will be important to adopt an algorithm of feature selection, in order to select the most discriminative features that permits to have a better overall performance.

# Conclusions

The goal of the present thesis is to implement an artificial neural network (ANN) in combination with an inertial sensors-based system, capable of estimate properly the vertical ground reaction forces during running.

It is a field of relevant interest in medical engineering and sport science since avoiding injuries related to running movements or improving sport performance is extremely important.

Accurate systems are available, but are expensive and constrained to lab-environments.

Recently, wearable motion sensors have been proposed as the solution which can guarantee a good trade-off between unobtrusiveness, low-cost, accuracy and versatility.

The developed system has been envisioned to be a low-cost alternative to the expensive instrumented treadmill or force platforms. A restrained number of IMUs were adopted (one per leg).

The inertial data (acceleration and radial velocity) were re-processed: a stride segmentation approach permitted to identify the time intervals between heel strikes and toe offs (e.g. contact time) has been implemented and afterwards several features were extracted from the data set segmented.

Due to the non-availability of force platforms or instrumented treadmill, the vGRFs target were generated by adopting Clark's method, namely a particular technique to simulate vGRFs.

Afterwards, the vGRFs were estimated from inertial data via artificial neural network algorithms, which have been used to find the correlation between the inertial measurements and the vGRFs target.

A number of ANN with an input layer, a single hidden layer and an output layer were designed; the activation function adopted of the hidden layer neurons was a sigmoid function while a linear one was adopted for the output layer. The number of neurons in the hidden layer of each network was different (increasing number, from 5 neurons until 100 neurons).

The method to find the most performant ANN was a Leave One Subject Out – Cross Validation (LOSO – CV). The type of results adopted of the validation were the Mean Absolute Error (MAE) and the Person Correlation Coefficient (R).

After each network has been validated, the most performant network was chosen in terms of lower MAE and higher R. The network chosen was finally tested with the test set.

The final results show the capability of this method to give a proper estimation of the vGRFs.

In conclusion, the present study proved that ANNs can be adopted to estimate GRFs in conjunction with motion sensors, which is a promising step towards the development of an accurate and low-cost objective assessment of running biomechanics on-the-field.

# Bibliography

[1] Erfan Shahabpoor, Aleksandar Pavic “Measurement of Walking Ground Reactions in Real-Life Environments: A Systematic Review of Techniques”, 1-7

[2] Davide Giovanelli, Aldo Rossi- Sistema di misura delle forze di contatto durante la corsa, 20-21

[3] "Motion Capture: Optical Systems". Next Generation. Imagine Media (10): 53. October 1995.

[4] Alessandro Sona Matteo Bertocco. “Introduzione alle misure elettroniche”. Lulu, second edition, Feb 2013, 12-30.

[5] Oliver J. Woodman. “An introduction to inertial navigation”. Computer Laboratory, Aug 2007. 9-17.

- [6] J. B. Kuipers. Quaternions and rotation sequences: A primer with applications to orbits, aerospace and virtual reality. 1999.
- [7] N. Yazdi, F. Ayazi, and K. Najafi. Micromachined inertial sensors. Proceedings of the IEEE. Aug 1998. 1640–1659.
- [8] Oliver J. Woodman. An introduction to inertial navigation. Computer Laboratory, Aug 2007. 107-115.
- [9] P. Cabena; P. Hadjinian; R. Stadler; J. Verhees; A. Zanasi. Discovering data mining from concept to implementation, Prentice Hall PTR 1997
- [10] Rota Bulò Samuel – “Appunti Reti Neurali”, 5-20
- [11] G. Balestra, S. Rosati – “Neural networks”, 15-26
- [12] D.C. Billing, C.R. Nagarajah, J.P. Hayes, J.Baker “Predicting ground reaction forces in running using micro-sensors and neural networks”
- [13] G.Leporace, L.A. Batista, L. Metsavath, J. Nadal, “Residual analysis of Ground Reaction Forces Simulation during Gait Using Neural Networks with different Configurations”
- [14] Frank J.Wouda, Matteo Giuberti, Giovanni Bellusci, Erik Maartens, Jasper Reenalda, Bert-Jan F.van Beijnum and Peter H.Veltink - “Estimation

of Vertical Ground Reaction Forces and Sagittal Knee Kinematics During Running Using Three Inertial Sensors”

[15] Yu Liu, Shi-Min Shih, Pei-Chin Guo – “Neural Network Used For the Prediction of Joint Torque from Ground Reaction Force During Counter-Movement Jump and Squat Jump

[16] Kenneth P.Clark, L. Ryan, P. Weyand “A general relationship links gait mechanics and running ground reaction forces”

# Ringraziamenti

Siamo giunti alla fine della tesi e di molte altre cose. I ringraziamenti sono forse la parte più importante di tutto ciò che ho scritto, perchè senza ogni singola persona che ho incontrato, non sarei qui ora, nel modo in cui lo sono ora.

Grazie ai miei genitori, a mamma e papà, due persone speciali che amo, i quali mi hanno sempre sostenuto ed hanno reso possibile in primis tutto ciò, partendo dal mio primo anno di ingegneria, sino a questa esperienza all'estero di grande valore.

Grazie ai miei parenti, i miei zii, ai miei nonni che mi hanno sempre coccolato, soprattutto mando questo grazie a mio nonno materno che è venuto a mancare poco prima che partissi per l'Irlanda, sono certo che in questo momento sarebbe super fiero di me.

Grazie alla mia ragazza, che nonostante tutte le difficoltà e le paure dovute dalla distanza che ci ha separati, mi ha sempre dato amore e forza per raggiungere gli obiettivi.

Grazie al professor De Marchi, Salvatore e Brendan. Il primo, oltre che ad essere stato mio professore durante i miei studi, mi ha dato la possibilità di intraprendere questa esperienza di ricerca, seguendomi ed essendo molto disponibile. Salvatore, la persona che mi ha seguito più da vicino durante questa esperienza di tesi, lo ringrazio per la sua professionalità e per tutto ciò che mi ha insegnato. Ringrazio Brendan per avermi accolto inizialmente in Tyndall con simpatia e vivacità.

Ringrazio tutte quelle persone che ho conosciuto a Cork, soprattutto il mio coinquilino tedesco Paul, ne abbiamo passate di cotte e di crude, lo ringrazio particolarmente per la sua presenza, i suoi consigli e per avermi reso questa esperienza irlandese ancora più ricca.

Ringrazio tutti i miei “compagni di scrivania”, da Davide a Marco per aver reso le mie giornate più divertenti e spensierate.

Grazie agli amici del politecnico, i quali hanno reso questo poli meno infernale con la loro simpatia rimanendo sempre presenti, in particolare grazie a Francesco, Simone, Bruno e Michele.

Grazie a tutti i miei amici di giù, in particolare le mie cugine Rosa e Santi, Leo, Loris e tutte le altre persone che hanno rappresentato qualcosa di importante durante questa fase della mia vita. Grazie di cuore a tutti, per tutto ciò che mi avete dato.